

2011
2012

GENEESKUNDE

*master in de biomedische wetenschappen: bio-elektronica
en nanotechnologie*

Masterproef

*Interfacing electrogenic cells with ultrathin layers of
graphene for sensor applications*

Promotor :
Prof. dr. Patrick WAGNER

Promotor :
prof. dr. SVEN INGEBRANDT

Lotta Delle

*Masterproef voorgedragen tot het bekomen van de graad van master in de biomedische
wetenschappen , afstudeerrichting bio-elektronica en nanotechnologie*

De transnationale Universiteit Limburg is een uniek samenwerkingsverband van twee universiteiten in twee landen:
de Universiteit Hasselt en Maastricht University



Universiteit Hasselt | Campus Diepenbeek | Agoralaan Gebouw D | BE-3590 Diepenbeek
Universiteit Hasselt | Campus Hasselt | Martelarenlaan 42 | BE-3500 Hasselt



2011
2012

GENEESKUNDE

*master in de biomedische wetenschappen: bio-elektronica
en nanotechnologie*

Masterproef

*Interfacing electrogenic cells with ultrathin layers of
graphene for sensor applications*

Promotor :
Prof. dr. Patrick WAGNER

Promotor :
prof. dr. SVEN INGEBRANDT

Lotta Delle

*Masterproef voorgedragen tot het bekomen van de graad van master in de biomedische
wetenschappen , afstudeerrichting bio-elektronica en nanotechnologie*

Abstract

Graphene as a conductive, transparent material, with a low cost and low environmental impact is reported to be ideal for sensor application. It is broadly investigated and promises an improvement of sensing performance due to its unique electrical transport properties. Therefore the use in active sensor elements such as ultrathin field-effect transistors for the detection of cellular signals is very novel. In this contribution the fabrication of ultrathin reduced graphene oxide (rGO) micropatterns via a soft lithography approach can be demonstrated using the Micro-molding in Capillaries (MIMIC) technique. Graphene oxide (GO) patterns with 5 to 50 μm width and less than 20 nm height were obtained. The GO patterns could be reduced to rGO via an environmentally friendly chemical route using L-ascorbic acid (L-AA). Cardiac myocytes (HL-1 cells) could be coupled to the micropatterned graphene lines, proliferation was studied and cell adhesion could be detected by impedance spectroscopy.

Abbreviations

L-AA	L-Ascorbic Acid
AFM	Atomic Force Microscopy
APTES	Aminopropyltriethoxysilane
CVD	Chemical Vapor Deposition
DNA	Deoxyribonucleic Acid
DI	De-Ionized
EIS	Electrochemical Impedance Spectroscopy
FBS	Fetal Bovine Serum
FET	Field Effect Transistor
FOCTS	Trichloro(1H,1H,2H,2H-perfluorooctyl)silane
GO	Graphene Oxide
MEA	Micro Electrode Array
MIMIC	Micromolding in Capillaries
MOSFET	Metal-Oxide-Semiconductor Field-Effect-Transistor
MTT	3-(4,5-Dimethylthiazol-2-yl)-2,5-diphenyltetrazolium bromide
PDMS	Poly(dimethylsiloxane)
rGO	reduced Graphene Oxide
RT	Room Temperature
SEM	Scanning Electron Microscopy
SiO ₂	Silicon Dioxide
XPS	X-ray Photoelectron Spectroscopy

Table of Contents

Abbreviations	III
1. Introduction	1
1.1. Motivation and state-of-the-art	1
1.1.1. Cell recordings	2
1.2. Objectives of the thesis	3
1.3. Fundamentals	3
1.3.1. Graphene materials, properties and fabrication methods . . .	3
1.3.2. Micromolding in capillaries	6
1.3.3. Electrophysiology of electrogenic cells	8
2. Materials and methods	11
2.1. Sensor fabrication	11
2.2. Physical characterization	15
2.2.1. Digital microscopy	15
2.2.2. Profilometry	15
2.2.3. Scanning electron microscopy	16
2.2.4. Atomic force microscopy	17
2.3. Electrochemical characterization	17
2.3.1. Impedance spectroscopy	17
2.4. Sensor functionalization with cardiac cells	20
3. Results and discussion	21
3.1. Sensor fabrication and measurement setup	21
3.1.1. Environmental-friendly reduction of GO by ascorbic acid . .	23

Table of Contents

3.2. Physical characterization	25
3.2.1. Digital microscopy	25
3.2.2. Profilometry	30
3.2.3. Scanning electron microscopy	32
3.2.4. Atomic force microscopy	34
3.3. Electrochemical characterization	36
3.3.1. Impedance measurements of rGO	36
3.3.2. Impedance measurements with functionalized sensors	38
3.3.3. Impedance measurements with non-adherent HL-1 cells	40
4. Conclusion and outlook	43
Bibliography	45
A. Appendix	49
A.1. Mask layout and protocol for mold fabrication	49
A.2. Technical drawings	52
A.3. Impedance spectra of reduced graphene oxide	54
A.4. Impedance spectra of cell functionalized sensors	57

1. Introduction

Nanocarbon materials have recently gained a big impact in biosensor development. They offer a simple detection scheme, high sensitivity and selectivity and a capability for real-time monitoring. Publications were dominated by molecular or chemical detection mechanisms. Recently graphene sheets were used for the detection of proteins, deoxyribonucleic acid (DNA) and the monitoring of gasses. Due to its sensing performance, low noise and cost-effectivity became more and more attractive in biosensing applications. The interface of graphene with living cells is said to be the future generation of neuroprosthetic devices [1]. It promises a further improvement of the signal detection capability, stability in biological environments and a higher compatibility with living tissue. Since conventional silicon technology mainly uses metal-oxide-semiconductor field-effect-transistors (MOSFETS) to interface living cells. But due to a limited stability in aqueous environments and a relatively high electrical noise, the focus on alternative materials was promoted. The integration of graphene electronics promises a breakthrough in the design of biomedical implants because of the facile integration of graphene with flexible substrates fulfilling an important requirement regarding to the reduction in tissue damage and scarring [2].

1.1. Motivation and state-of-the-art

Graphene as a zero-band-gap [3] atomic monolayer of graphite, consisting of a planar sheet of sp^2 -bonded carbon atoms has been identified to be a promising material for electronic sensor applications. Due to its unusual properties like extremely high charge carrier mobility, chemical stability, biocompatibility and flexibility, graphene immediately became an objective in nanomaterials research. It shows great application possibilities in various sensor devices based on nanowire field-effect-transistors (FET), carbon nanotubes and recently single graphene sheets [4]. Since the first

1. Introduction

isolation of free standing graphene in 2004 [5] the 2-dimensional material has been utilized as a transducer in many sensor devices such as bio-field-effect transistors, electrochemical biosensors, impedance biosensors, electrochemiluminescence and fluorescence biosensors [6]. Transducing systems for biosensing are mostly piezo-electric, optical or electrochemical. Biosensing devices are required to be portable, economically accessible and unsusceptible to cross contamination.

Electrochemical impedance spectroscopy (EIS) is a sensitive, label-free technique that is ideally suitable for a graphene platform. For impedimetric sensing a transducer with a high conductivity, high electron mobility and a large area for the biorecognition layer is preferable. Nanostructured materials with a high surface-to-volume ratio were recently used for impedimetric detection due to their exceptional properties. Graphene and graphene-derived materials, like rGO, exhibit metallic conductivity, high electron transfer-rates and a large surface area [7]. Therefore graphene represents a suitable transducer material for the investigation of interfacial properties by EIS. Impedance spectroscopy is also used for effect monitoring. It implements a method for the investigation of metabolic activity, response to potential drugs, for cytotoxicity tests and cell adhesion on surfaces [8] [9] [10] [11]. An impedimetric detection of cell adhesion is represented in this thesis.

For further applications electrical signals generated by electrogenic cells undergoing a transient depolarization and repolarization that can be triggered by external mechanisms or intracellular spontaneous mechanisms can be recorded. Most common electrogenic cells are neurons (brain cells) or cardiomyocytes (heart cells).

1.1.1. Cell recordings

Coupling biological elements with microelectronic devices leads to electronic hybrid devices, steering towards high sensitivity and selectivity of biological detection mechanisms. In combination with advanced signal amplification methods and processing, those systems allow to investigate the fundamentals of functionality in cellular networks and signal propagation. Standard electrophysiological measurements were performed by metal electrodes or microelectrodes pulled from glass capillaries. This technique known as patch-clamp, was developed in 1976 by Erwin

1.2. Objectives of the thesis

Neher and Bert Sakmann to study single ion channels in the biological membrane. The setup consists of a glass pipette filled with electrolyte and an electrode inside. The pipette is attached to the membrane and a vacuum is applied. Therefore the membrane can be manipulated and characterized in different configurations i.a. to study single ion channels. The advantage of intracellular measurements is a very good signal to noise ratio, but due to the fact that they are invasive and limited to only a few cells, extracellular recording with micro electrode arrays (MEAs) [12] and FETs [13] gain more and more popularity.

1.2. Objectives of the thesis

In this work an interface of electrogenic cells with micropatterns of graphene will be described in order to allow for cellular recordings.

Graphene oxide micropatterns were fabricated via a soft lithographic approach 'micromolding in capillaries' (MIMIC) and a suitable reduction route to reduced graphene oxide was established. The patterns have been characterized physically and were electrically contacted using metal deposition through a shadow mask. The electrical transport properties of the devices were investigated and they have been operated in a liquid environment. In the second part of the thesis, cardiac myocytes were cultured on the devices and cellular recordings were performed.

1.3. Fundamentals

The following sections deal with a summary about the basic matter of graphene and its properties, the reduction of GO, the used soft lithography technique and fundamental issues about the signal propagation of electronic cells in order to give an introduction to this interdisciplinary field.

1.3.1. Graphene materials, properties and fabrication methods

Carbon compounds, such as the elementary component of diamond and graphite, form the molecular basis of all life on earth. Since different carbon allotropes have

1. Introduction

been reported like three-dimensional graphite, two-dimensional graphene, one-dimensional nanotubes and zero-dimensional fullerenes (see figure 1.1) new properties and applications have been investigated.

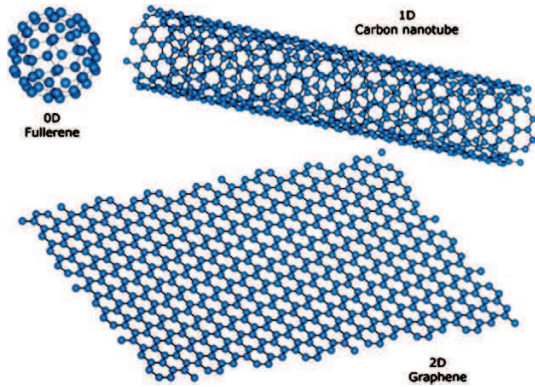


Figure 1.1.: Different carbon allotropes [14].

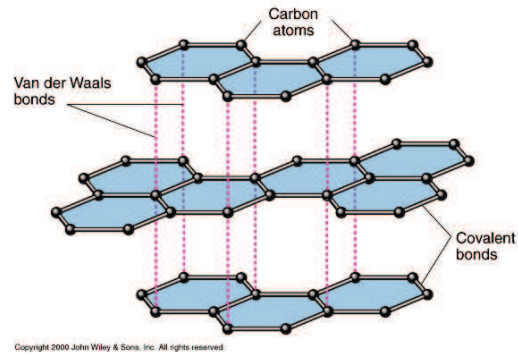


Figure 1.2.: Stacked graphene single layers [15].

After the isolation and characterization of the first graphene monolayers by NOVOSELOV ET AL. in 2004 [5] scientists all over the world investigated the properties of the exceptional material. Graphene is a one-atom thick sheet of graphite consisting of sp^2 -bonded carbon atoms arranged in a two-dimensional honeycomb lattice. It is considered to consist of stacked monolayers (number < 10) on top of each other, differentiated into mono-, bi- and multi-layers [16]. More than 10 layers refer to graphite thin films. Each layer has a carbon-to-carbon bond length of about 0.142 nm [2] and an angle of 120° . The interlayer spacing of stacked layers amounts to 3.34 Å interconnected through van-der-Waals forces (see figure 1.2). Each carbon atom has one s-orbital and two p-orbitals, that are in-plane leading to a high mechanical stability. Known as the strongest material, graphene has an elastic stiffness of 340 N/m and a Youngs modulus of 1 TPa. The remaining p-orbital is perpendicularly oriented to the molecular plane and hybridizes to form the π^* (conduction) and π (valence) bands dominating the planar conduction properties.

The electrical properties of graphene can be described by the Tight-Binding-Model, which is used to calculate the band structure of solids and molecules. Figure 1.3 shows the band structure of graphene. It differs considerably from the band structure in semiconductors. This is caused by the linear dispersion relation $E(k)$ of electrons near the K-point of the hexagonal Brillouin zone, where conduction and valence

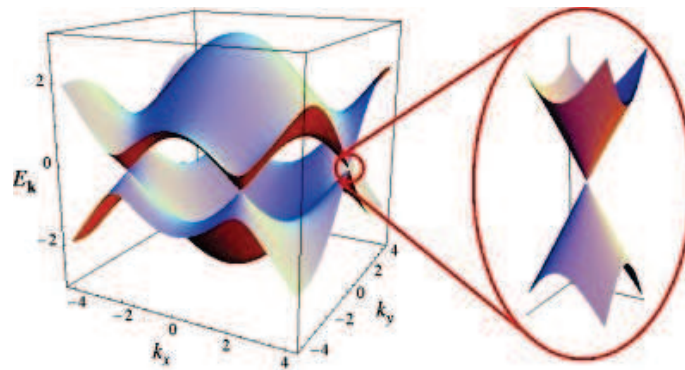


Figure 1.3.: Bandstructure of Graphene [16].

band are touching, cone-shaped structures called the Dirac cones are formed. They are touching in exactly six points, the so called K-points, corresponding to the six corners of the honeycomb lattice. The relationship between momentum and energy close to these points is linear, so that electrons behave approximately as particles without mass. That means by applying an electric current to a graphene sheet in this state the mean free path corresponds to 700 atoms. Moving without scattering the electrons reach a speed of 10^6 m/s.

Graphene can be fabricated by three different main methods including mechanical exfoliation, supported growth and colloidal suspensions. Mechanical exfoliation or the "Scotch-tape-method" was developed during the discovery of single graphene sheets by NOVOSELOV ET AL. This is performed by peeling a graphitic substrate with an adhesive tape. The stick and peel process is repeated for a dozen times, bringing a $1\ \mu\text{m}$ thin graphite flake to a monolayer. The disadvantage of this method is that mechanical exfoliation has a low throughput and is not applicable for large-size production. Supported growth of graphene on solid substrates includes chemical vapor deposition (CVD) and thermal decomposition of silicon carbide to graphene at high temperatures. CVD growth of graphene on a copper foil is a self-limiting process, because the growth stops automatically, after a single graphene layer is formed. Advantages of CVD are the possibility of substitutional doping and the ability to grow large-sized graphene films. However, CVD lacks in the quality of the graphene layer due to the existence of defects, impurities and the difficulty to transfer the grown layer from the metal to an insulating substrate. The decomposition of silicon carbide at high temperatures has the advantage that

1. Introduction

the transfer process of the graphene sheet is not required because the substrate itself is insulating. Therefore it is a good method for the production of large integrated circuits. The growth itself is not self-limiting, as a result the graphene film is not homogeneous.

The production of graphene by colloidal suspensions of exfoliated GO was historically the first method of graphene synthesis, published by BOEHM ET AL. [17] already in 1962. Graphene oxide is fabricated by the oxidation of graphite with strong reactants and subsequent dispersion in solvents in order to obtain a GO solution. A lot of different ways were established for the reduction of graphene oxide. The reduction will be discussed in more detail in chapter 3.1.1. This method is very suitable for the low-cost mass production of reduced graphene oxide.

1.3.2. Micromolding in capillaries

The usual technique to create patterns in microfabrication is photolithography or electron beam lithography. During a photolithographic process a photomask is projected onto a photoresist via UV-light, followed by the development of the resist, lift-off procedure and etching of the substrate. Electron beam lithography is performed via the scanning of a resist film with an electron beam. Both techniques are very suitable for the fabrication of small structures, but photolithography is dependent on the wavelength of the incident light for the projection of the mask and therefore limited in resolution. Complex equipment is needed as well and therefore also the economical viability is also limited.

Taking this into account, a different lithography method was developed by XIA AND WHITESIDES ET AL. in 1990 [18] called soft lithography. The key component in soft lithography is a soft polymer stamp with a relief structure used for printing or molding a pattern on top of a substrate. The stamp consists of cross-linked silicone mostly poly(dimethylsiloxane) (PDMS). The substrate in many microelectronic fabrication methods is silicon. It is used as a substrate for the patterns as well as a master for the stamp fabrication. Glass substrates are also possible, if silicon as a semiconductor is not suitable. Stamp fabrication is done by using a structured silicon wafer as a master. A prepolymer is poured over the master's relief structure, cured and peeled off, patterned by the negative relief structure of the master.

1.3. Fundamentals

Chemical modifications of the substrates surface are crucial for soft lithography. When the polymeric stamp gets in contact with the substrate by molding, both components stick together due to their surface properties. Therefore a release agent for the separation of stamp and substrate is needed. Modification of the substrates surface with organosilanes in a self-assembling process helps to lower the surface energy of the substrate. Micromolding in capillaries is one of the soft lithography techniques developed by WHITESIDES ET AL. in 1995. It uses a mold (PDMS stamp) that is placed on top of a substrate with a relief of line structures on the bottom part forming channels between stamp and substrate. At the open ends of the channel a liquid is placed (e.g. GO solution) filling the channels by capillary action. After drying the GO solution and removing the stamp, patterned GO lines are left on the substrate (principle see figure 1.4). MIMIC provides an fast way to obtain patterned GO structures in the μm range. It is straight forward, cost-effective and does not require any special equipment. For these reasons it was chosen for this work.

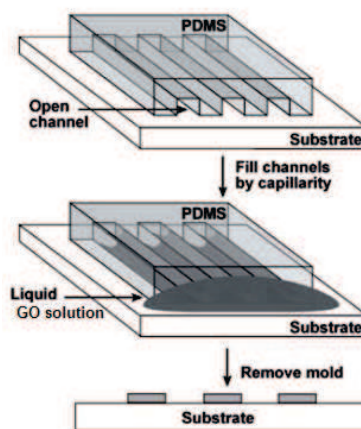


Figure 1.4.: Principle of micromolding in capillaries [19].

The filling of a cylindrical capillary with liquid is caused by the interfacial tension. The capillary effect induces wetting liquid rising against gravity to the top (capillary ascension). Figure 1.5 shows a schematic sketch of the capillary effect including the variable used for the following derivation of the maximum rise of liquid. In a capillary with diameter $d = 2r$ and an ideal contact angle of $\delta = 0$ the curvature

1. Introduction

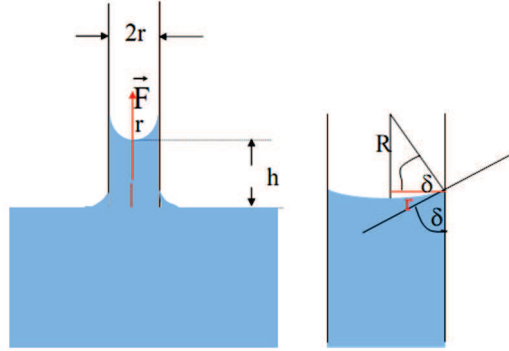


Figure 1.5.: Schematic of the capillary effect [20].

of the rising liquid is exactly r . The curved surface generates an upward pressure by the amount of $p = 2\gamma/r$, with γ equal to the surface tension, resulting in the surface of the capillary πr^2 into an upward force: $F = p\pi r^2 = 2\gamma\pi r$. At the same time, the force of gravity acts on the water column: $mg = \rho h\pi r^2 g$ with ρ as the density of the liquid, h as the maximum rise of the liquid and the gravity g . Due to the equilibrium condition $F = mg$ one can calculate the maximum rise of the liquid inside the capillary:

$$h = \frac{2\gamma}{r\rho g} \quad (1.1)$$

For a small capillary diameter e.g. $20\ \mu\text{m}$, h can reach a notably value of $1.40\ \text{m}$ for the surface tension of H_2O . If the contact angle is $\delta > 0$, the radius of the curvature R of the column decreases and thus also the height of the rise. The pressure is now defined as $p = 2\gamma/R$ and with $r = R \cos \delta$ the rise of the height is:

$$h = \frac{2\gamma \cos \delta}{r\rho g} \quad (1.2)$$

1.3.3. Electrophysiology of electrogenic cells

Cells are considered to be the basic units of life. Each cell has a semipermeable membrane consisting of a phospholipid bilayer that separates it from the environment. The membrane controls the transport of molecules inside the cell by transport proteins or diffusion, but its key role is to maintain the cell potential by ion channels. Ion channels are responsible for the voltage gradient existing across the membrane of all living cells. They establish and control the voltage gradient across the mem-

1.3. Fundamentals

brane. Due to an inhomogeneous distribution of ions the cell forms a membrane potential between the inside of the cell and the surrounding liquid. The membrane potential has a value of -60 to -90 mV. The concentration difference of specific ions like sodium and potassium is achieved by a number of specific sodium-potassium pumps (Na-K-ATPase) scattered across the cell membrane. For each conversion cycle of ATP into ADP two potassium ions are pumped into the cell while three sodium ions are pumped out. In this way a distribution of positively charged ions across the cell membrane is reached. In this distribution more sodium is present outside the cell than inside and the other way around for potassium.

An expression for the membrane potential assuming a system in thermodynamic equilibrium is the Nernst equation (1.3) for K^+ ions,

$$E_m = \frac{R \cdot T}{z \cdot F} \cdot \ln \frac{[K^+]_o}{[K^+]_i} \quad (1.3)$$

with gas constant R (8.31 J/mol K), temperature T , Faraday constant F ($96.5 \cdot 10^3$ C/mol) and the charge of the ion z . Equation 1.3 only includes the K^+ ions, but the cell membrane is permeable for Na^+ and Cl^- ions as well. All major ions permeabilities (P_x) are included in the Goldman equation (1.4) to calculate a more exact resting potential.

$$E_m = \frac{R \cdot T}{F} \cdot \ln \frac{P_K \cdot [K^+]_o + P_{Na} \cdot [Na^+]_o + P_{Cl} \cdot [Cl^-]_i}{P_K \cdot [K^+]_i + P_{Na} \cdot [Na^+]_i + P_{Cl} \cdot [Cl^-]_o} \quad (1.4)$$

Like the resting potential described in equation 1.4, also action potentials depend on the permeability of the cell membrane to Na^+ and K^+ ions. An action potential is considered to be a change of the membrane voltage (V_m) over time. When a specific threshold is reached, the voltage-gated Na^+ channels are opening and a positive ion current flows into the cell (depolarization). With a little delay a positive potassium current flows out of the cell. At the same time Na^+ channels close and V_m reaches a maximum value. The continuous potassium outflow leads to a decrease of the membrane potential, called repolarization. Even a drop of V_m to a lower value than the initial resting potential (V_{rp}) is possible (hyperpolarization). A final action of the above mentioned sodium-potassium pumps restores the original V_m . Excitable or electrogenic cells are nerve- or muscle-cells, because they are able to rapidly change their membrane potential by gated ion channels dependent

1. Introduction

on voltage or ligands. Their most important function is the propagation of action potentials (see figure 1.6).

For the recording experiments described in this thesis, HL-1 (human leukemia)

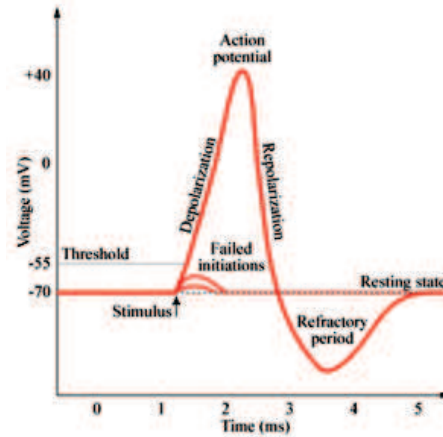


Figure 1.6.: Phases during the propagation of an action potential [21].

cells were used. HL-1 cells were successfully derived by Claycomb et al. [22] in 1998 from a mouse cardiomyocyte tumor cell line in order to create a cell line that provides the characteristics of adult cardiac muscle cells. The cell line exhibits contractile behaviour by spontaneous depolarization and the expression of the necessary ion channels for generating action potentials. HL-1 cells can be passaged in culture as well as recovered from frozen stocks. Due to the fact that the cells are easy to culture and show spontaneous electrical activity, they are a promising candidate for signal recording experiments and cell-chip coupling.

2. Materials and methods

The following chapter describes the fabrication of the sensor device, which is the central focus of this work. Single process steps are explained and an overview on the different physical and electrochemical sensor characterization techniques is given. Subsequently the sensor functionalization with cardiac cells is briefly described.

2.1. Sensor fabrication

The sensor chips were fabricated in different steps by the following procedure illustrated in figure 2.1. The following enumeration refers to each step and states the protocol of the sensor fabrication.

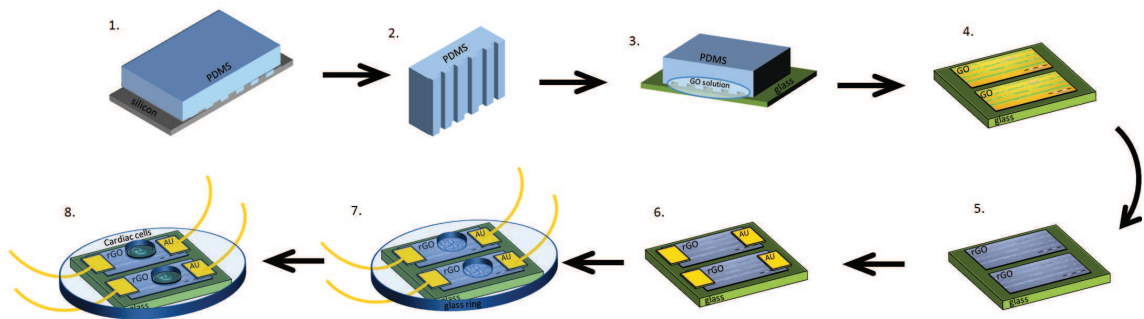


Figure 2.1.: Fabrication of reduced graphene patterns contacted with gold pads on a glass substrate, encapsulated and functionalized with cardiac cells.

- 1. Production of the patterned PDMS stamp:** A negative silicon mold was fabricated by photolithographic steps (protocol see appendix section A.1). The wafer was silanized with Trichloro(1H,1H,2H,2H-perfluorooctyl)silane (FOCTS) (Sigma Aldrich, Germany) creating a hydrophobic surface to achieve a better release of the produced PDMS stamp. This is caused by non-reactive

2. Materials and methods

CF-groups on the wafer surface. Before the silanization step the surface of the wafer needs to be activated in oxygen plasma (Diener electronics, Germany) (0.6 mbar; 140 Watt; 1 min). The silanization takes place in a glovebox with nitrogen atmosphere. The wafer was placed in a desiccator inside the glovebox together with 20 μ l of FOCTS. The silanization was initiated by the evacuation of the desiccator to 40 mbar. After the functionalization of the negative silicon master, a PDMS stamp was fabricated with Sylgard 182 kit (Dow Downing), consisting of a base and a curing agent. Both agents were mixed in a 1:10 ratio and stirred for 5 min in a glass beaker with a glass stick. The liquid PDMS was degassed in vacuum in a desiccator for 1.5 h and casted onto the negative silicon wafer, which was fixed in a holder. The PDMS in the holder was degassed a second time for 1 h and cured in the oven for 2 h at 80 °C and 2 h at 120 °C.

- 2. Peeling off the stamp:** The hardened PDMS stamp on the negative silicon master was cooled down till the wafer with the PDMS could be released out of the holder. The PDMS stamp was peeled off carefully from the wafer using tweezers and stored with the patterned structure at the top on a flat surface covered with a lid. The PDMS stamp with different structures was cut in 3 x 7 mm pieces patterned with the desired size of the structure. The PDMS stamp was prepared by plasma activation of the patterned side at 0.6 mbar and 140 Watt (70% of 200) for 1 min in order to create a hydrophilic surface. After the activation the stamp needs to be stored for 3 h to reduce the effect of the plasma activation.
- 3. Micromolding in capillaries:** Required for the MIMIC procedure is the silanization of the 1.3 x 1.3 mm² glass chip surface with 3-Aminopropyltriethoxysilane (APTES) (Sigma Aldrich, Germany) in order to produce a hydrophobic surface with covalently bound amino groups. Before the silanization the chip surface needed to be cleaned in Acetone (Sigma Aldrich, Germany) (15 min), Propanol (Sigma Aldrich, Germany) (15 min) and DI-water (15 min) in an ultrasonic bath (Bandelin Sonorex, RK 100, Germany). After that, the surface of the chips was activated in oxygen plasma in order to create reactive hydroxyl groups enabling the silanization process. The acti-

2.1. Sensor fabrication

vation was done at 0.6 mbar and 140 Watt for 1 min. Immediately after the activation the chips were moved into a glovebox with a nitrogen atmosphere to perform the process in a gas-tight oxygen-free environment. The silanization with APTES includes two preheating steps at 200°C for 1h each to bring the desiccator and the sample holder to the appropriate temperature (protocol for silanization see reference [23]). After heating up the equipment, the chips to be silanized are placed in the desiccator together with 200 µl of APTES and the silanization was performed for 1.5 h at 150 °C. The GO solution was prepared with a GO concentration of 2 mg/ml in DI-water by sonication in an ultrasonic bath (ELMA Transsonic digital, T 680 DH, 40 kHz, 150 Watt, USA) for 6 h to break the GO flakes (Graphene supermarket) and disperse them into the solution. The MIMIC procedure was performed by aligning the activated PDMS stamp on the dust free surface of the silanized glass chip with the patterned structure of the stamp being in contact with the chip surface. A 5 µl drop of GO solution was placed at the open channels of the stamp. Due to the capillary effect the GO solution was sucked into the patterned lines of the stamp.

4. **Release of stamp:** After performing the casting of the drop the chips with the stamp and GO solution were placed in a desiccator for 20 min in order to strengthen the filling of the channels inside the vacuum and dry the GO solution. After drying the solution the stamp can be peeled off the chip surface carefully with tweezers. Due to the silanization, no PDMS should stay attached to the surface of the chip.
5. **Reduction of GO patterns:** The reduction of the patterned GO lines was performed on-chip by a solution of L-AA (Riedel de Haen, Germany) with a concentration of 5 mg/ml at room temperature. The patterned chip was stored in 4 ml of the L-AA solution for 4 days. The reduction took place due to the substantial removal of oxygen functionalities in the GO. After the storage in L-AA solution the chip was dried under a nitrogen pistol with low pressure and left in the oven for 30 min at 100 °C to remove residual water.
6. **Contacting of rGO patterns:** The rGO patterns were contacted by gold deposition through a shadow mask (3000 Å, 5 Å/s, power 51 %) A metallic mask

2. Materials and methods

for the contacting of 16 chips with two sensors, i.e. four contacts on each chip was designed (see figure 2.3(a) and technical drawing A.4 and A.5 in appendix). The contacts were dimensioned with a $2 \times 4.5 \text{ mm}^2$ area and a height of 300 nm (see figure 2.3(b)).

7. **Encapsulation of rGO chips:** The chips were encapsulated with liquid PDMS filled in between a small (diameter: 3 mm) and a big glass ring (diameter: 18 mm) on top of the rGO patterns, so that just the area of the small glass ring (4.7 mm^2) stayed uncovered. The contacts were connected to copper wires via silver glue and also covered with PDMS to make sure that no short cut appears while measuring in buffer or culture medium (see figure 2.2). Additionally a measurement cell was designed for the electrical characterization of the sensor chips (see figure 3.1 and technical drawing A.2 and A.3 in appendix)
8. **Functionalization with cardiac cells:** Cardiac HL-1 cells were cultured on top of the encapsulated sensors inside the inner glass ring being in contact with the rGO lines. The glass ring was filled with Claycomb (Sigma Aldrich, Germany) medium and measurements could be performed using an Impedance analyser (Ivium CompactStat, Ivium Technologies BV, The Netherlands).

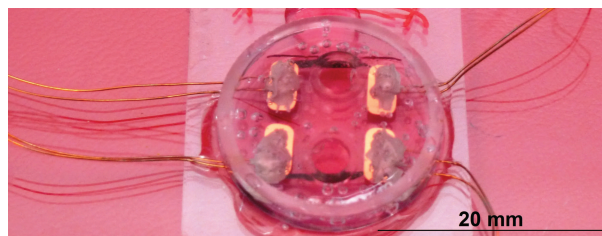
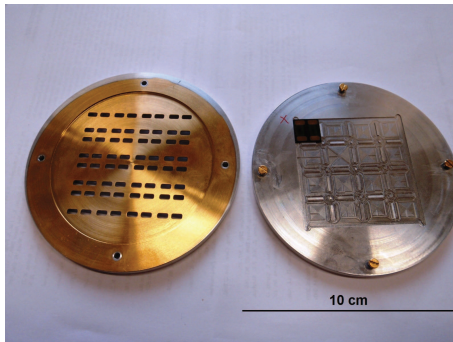
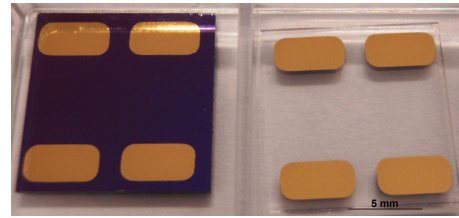


Figure 2.2.: Encapsulated sensor device.

2.2. Physical characterization



(a) Mask for the evaporation of gold contacts.



(b) Silicon and glass chip structured with gold contact.

Figure 2.3.: Fabrication of gold contacts.

2.2. Physical characterization

2.2.1. Digital microscopy

Light microscopy is used for magnification of small, for the human eye non-visible structures utilizing optical effects. The basic structure of a light microscope consists of the microscope base, the stage, coarse or fine adjustment knob to focus the preparations, the ocular lens and the objectives. Digital microscopes have the advantage that image data can be processed almost at the same time (no waiting time as in analogue cameras), which is realized with the help of a CCD matrix (Charged Coupled Device). In addition the image can be viewed simultaneously by multiple people. In this project digital video microscopy was used for the examination of graphene patterns on the chip surface using the DIC (differential interference contrast) mode.

2.2.2. Profilometry

Profilometry is a technique to study the surface topography of a sample. Here comes a diamond needle into use, scanning the surface and creating a surface profile of the sample. Profilometry is very suitable for the determination and analysis of step heights and micro roughness. The sample to be measured should not be too soft and should not have big surface distances. The advantage of profilometry is to get a relatively high content of information about the surface topography in short time. Additionally there is no need to prepare the sample before starting the measurement.

2.2.3. Scanning electron microscopy

In a scanning electron microscope (SEM) an electron beam is guided in a certain pattern over the surface of a sample. Due to interactions of the samples surface with incident electrons an image of the scanned object can be created. Images created by a SEM normally have a great depth of field. The electron beam is generated in an electron source. The electron source in simple devices is a tungsten wire which is heated up and emits electrons (a so-called thermionic cathode), which are accelerated in an electric field with a voltage of typically 8 to 30 kV. The electron beam in more advanced and costly devices are generated by field emission of tungsten single crystal emitters or the thermally assisted Schottky type, using emitters of zirconium oxide. A field emission gun consists of a very fine tip out of which electrons are tunneling out by applying a high electric field strength. A distinction is made between cold field emission, where the electrons escape from the tungsten tip due to the applied electric field and thermal field emission, where a Schottky cathode is heated slightly.

Thermal field emission has the advantage of an increased beam intensity because electrons have a more defined acceleration. The scanning process takes place in a high vacuum chamber to avoid interference with molecules and atoms in the air. Using magnetic coils the electron beam is focused on one point on the objects surface. Information about the image is obtained by different interactions of the electrons with the sample. Most of the information is gathered by an interaction of the primary electrons from the generated beam with the atoms of the samples surface. In this process secondary electrons are generated. Because of their low energy they can only come from the first few nanometers of the surface and give therefore information about the topography of the sample. More qualitative information can be obtained by the detection of backscattered electrons. The intensity of the signal is dependent on the atomic number of the material. Heavy elements provide a strong backscattering, therefore that corresponding element appears white. Areas with lighter elements appear darker. This allows also conclusions about the components of the object. Characteristic x-rays are often used to characterize small areas of the sample. Characteristic x-rays occur when an electron from the incident beam removes a core-level electron from its position. The position is filled by an electron from a higher orbital and the difference in energy is released in form of an x-ray

photon. The resulting x-ray radiation is characteristic for the electron shell of the atom and contains information about the element.

2.2.4. Atomic force microscopy

Atomic force microscopy is used for mechanical scanning of surfaces and the measurement of atomic forces on the nanometer scale. The so-called cantilever, a nanoscopically small needle attached to a leaf spring, is guided line by line in a defined grid over the surface of a sample. In this way the cantilever scans the surface of a defined area. The structure of the surface bends the leaf spring thereby in a different extent depending on the roughness of the sample. This bending or deflection of the tip can be measured by optical and capacitive sensors and is defined by atomic forces between the surface and the tip. Apart from attractive forces like van-der-Waals or capillary forces, there are strong repulsive forces. They can be quantummechanically described and are based on the Pauli principle and Coulomb repulsions of the atomic charges. By recording the deflections and forces in every point, an image of the sample's surface can be created. This way each pixel represents a physical or chemical measure. The resolution of the image is mainly determined by the radius of curvature of the tip (usually 10-20 nm). This allows a lateral resolution of 0.1 - 10 nm depending on the roughness of the surface.

2.3. Electrochemical characterization

2.3.1. Impedance spectroscopy

Impedance spectroscopy is a technique to investigate interfacial properties of conductive or semi-conductive surfaces. A sinusoidal, small-amplitude signal is used to understand electrical properties of materials. A measurement is performed by an impedance analyzer generating a time-dependent perturbation signal, a sinusoidal voltage, applied between two electrodes (sensing and working electrode connected together as well as counter and reference electrode connected together) for a certain range of frequency:

$$E_t = E_0 \cdot \sin(\omega \cdot t) \quad (2.1)$$

2. Materials and methods

where E_t is the potential at time t , E_0 is the amplitude of the signal, $\omega = 2\pi f$ is the radial frequency and f is the frequency expressed in Hertz (Hz). The current response of the signal is measured:

$$I_t = I_0 \cdot \sin(\omega \cdot t + \phi) \quad (2.2)$$

with I_t as the time-dependent current intensity, I_0 the amplitude of the signal, $\omega = 2\pi f$ is the radial frequency and ϕ the phase angle between E_t and I_t . The impedance of the system influences amplitude and phase angle of the obtained current (2.2). Analogous to Ohm's law it is possible to calculate the impedance of the system:

$$\frac{E_t}{I_t} = \frac{E_0 \sin(\omega t)}{I_0 \sin(\omega t + \phi)} = Z_0 \frac{\sin(\omega t)}{\sin(\omega t + \phi)} \quad (2.3)$$

The impedance is therefore expressed as the ratio of the applied signal and the response obtained in terms of Z_0 and a phase shift ϕ . In terms of Eulers relationship the impedance can be expressed as a complex function:

$$\exp(j\phi) = \cos \phi + j \sin \phi \quad (2.4)$$

Describing the potential as,

$$E_t = E_0 \exp(j\omega t) \quad (2.5)$$

and the current response as,

$$I_t = I_0 \exp(j\omega t - \phi) \quad (2.6)$$

the impedance can be represented as a complex number:

$$Z(\omega) = \frac{E}{I} = Z_0 \exp(j\phi) = Z_0(\cos \phi + j \sin \phi) \quad (2.7)$$

Measured data are either presented as a Nyquist plot or as a Bode diagram (see figure 2.4). The expression for $Z(\omega)$ in equation 2.7 consists of a real and an imaginary part. Plotting the real part on the x-axis and the imaginary part on the y-axis a Nyquist plot can be constructed. Here the impedance is represented as a vec-

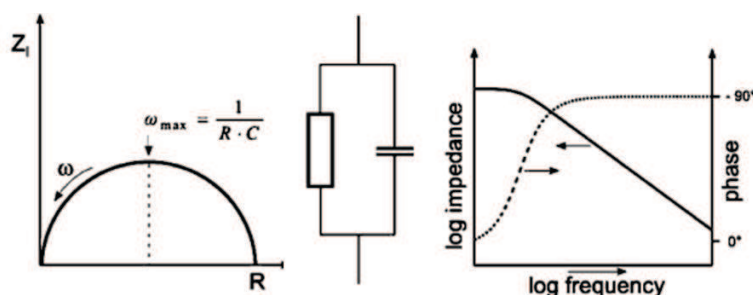


Figure 2.4.: Nyquist (left) and Bode (right) plot of a parallel circuit of a capacitance and a resistance [24].

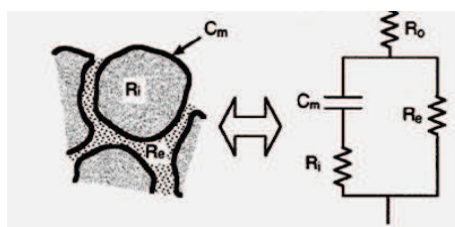


Figure 2.5.: Equivalent circuit modeling the key parameters for the impedance of a cell layer [24].

tor of length $|Z|$ and the phase angle is defined between the vector and the x-axis. The Nyquist plot does not give information on the frequency used for recording the data point. The Bode plot on the other hand shows frequency information. The impedance is plotted with the logarithm of the frequency on the x-axis and the absolute impedance values and the phase shift on the y-axis. Experimental impedance data can be approximated by an ideal circuit. Many electrochemical systems have been analyzed by this procedure and published in literature. Figure 2.5 shows a simplified equivalent circuit for the impedance of a cell layer being a parallel circuit of intracellular and extracellular pathways. The cytoplasm of the cell and the extracellular space are considered to be conductive media that is isolated from each other by the cell membrane. Therefore the conductivity of the extracellular space and the cell cytoplasm represent the resistive components for the internal (R_i) and external (R_e) charge carrier transport and the solution resistance (R_s) and cell membrane represents the capacitive effect (C_m).

2. *Materials and methods*

2.4. Sensor functionalization with cardiac cells

HL-1 cardiomyocytes were cultured and maintained in the incubator at 37 °C in humid atmosphere with 5 % CO₂ / 95 % air. For standard culturing conditions Claycomb medium (Sigma Aldrich) was used, containing 10 % fetal bovine serum (FBS) (v/v) (PAN), penicillin (100 U/ml) (PAN), norepinephrine (0.1 mM) (Sigma Aldrich), L-glutamine (2 mM, PAN). Encapsulated sensor devices were used for culturing HL-1 cells on top of the rGO pattern. Therefore the sensor chips were sterilized for 30 min under UV light and 100 µl of cell suspension was added on top of every device. After 4 hours the cells were settled down and the encapsulated chips were covered with 1 ml Claycomb medium. The medium was changed every day after the measurement was performed.

3. Results and discussion

The results obtained during the sensor fabrication and characterization with physical and electrochemical techniques are described and discussed in the following section.

3.1. Sensor fabrication and measurement setup

Next to the sensor development the concept of a stable measurement setup and the recording of the measurement signal for the readout system is very important. The fabricated sensor chips need a design that facilitates the electrochemical characterization in terms of checking the functionality and generating comparable measurement conditions for each sensor e.g. in a measurement cell. The chip design is based on the principle of a differential measurement between two sensors on each chip. Two blocks of a defined number of GO lines with a length of 7 mm were patterned via MIMIC next to each other on a silanized glass chip with an area of 1.3 x 1.3 cm². In order to contact the GO lines after reduction with gold contacts a metal mask was developed (see figure 2.3(a) and technical drawing in appendix (figure A.4, A.5)). The mask consists of two parts: The lower part is structured with 16 pockets in a square keeping the rGO patterned chips in place. The upper part of the mask covers the chip area of all 16 chips, but contains four windows for each chip to obtain a size defined gold contact (2 x 4.5 mm²) at the beginning and the end of the rGO lines via the evaporation of gold through the windows of the mask. The characterization of the obtained gold pads follows in chapter 3.2.

For the electrochemical characterization measurements were performed in a measurement cell, which was adapted to chip size and contact points. The measurement cell consists out of two parts. The chip is kept in place by a pocket located in the lower part of the measurement cell. When both parts of the measurement cell are

3. Results and discussion

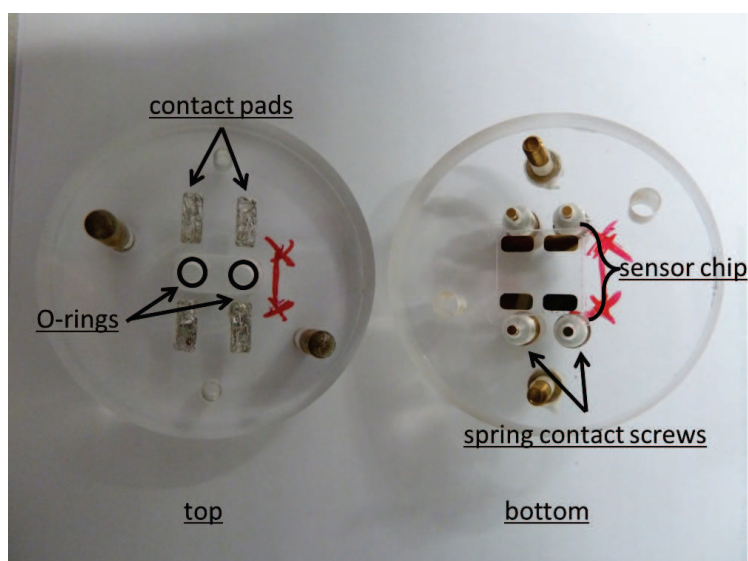


Figure 3.1.: Designed measurement cell for electrical sensor chip characterization.

interlocked, the gold pads on the chip are in contact with aluminum pads from the top part of the cell. Special screws with spring contact pins at the end touch the aluminum pads from the bottom part of the cell being able to be connected with 2 mm banana plugs. The upper part of the cell contains a hole with two separated chambers opening the sensitive surface of both sensors on each chip. The chambers are sealed with an O-ring in order to perform measurements in liquid (e.g. cell culture medium).

Sensors that could be characterized successfully were chosen for encapsulation. In order to culture cells on the rGO lines, the encapsulated device needed to be sterilized under UV light. The measurement cell was not applicable for sterilization and only the encapsulated chips could be characterized under the microscope, so that the measurement cell was mainly used for impedimetric characterization of the device before cell culture. The impedance measurements were performed inside a Faraday cage. The impedance analyzer was connected to the measurement cell via banana plug electrodes and the signal was processed by readout software on a laptop (see figure 3.2).

3.1. Sensor fabrication and measurement setup

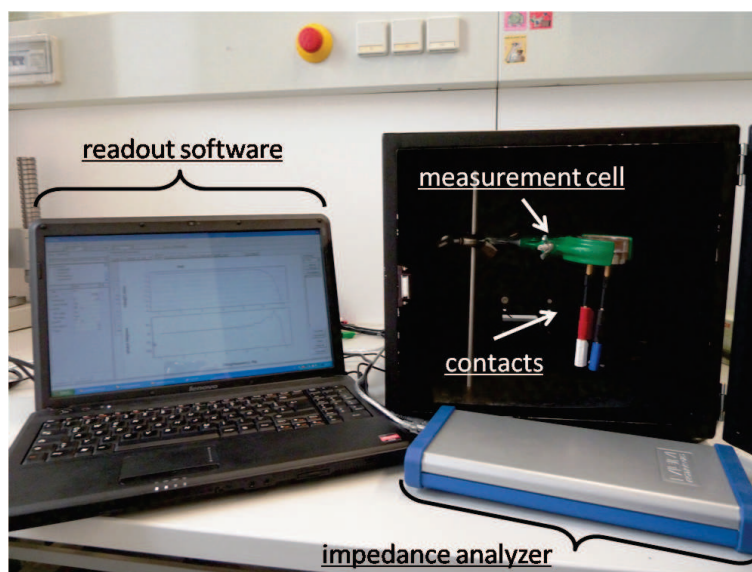


Figure 3.2.: Measurement setup.

3.1.1. Environmental-friendly reduction of GO by ascorbic acid

Graphene oxide is generally obtained with Hummers method by reacting graphite with a mixture of potassium permanganate ($KMnO_4$) and concentrated sulfuric acid (H_2SO_4) [25]. GO is a non-conductive, atomically thin sheet with nano-sized sp^2 carbon clusters isolated by oxygenated sp^3 carbon domains (see figure 3.3) By reducing GO chemically, thermal or electrochemically, it can be transformed from an insulator to a semi-conductor (rGO) due to the opening of epoxy bridges and the removal of the hydroxyl groups.

Reduced graphene oxide is very similar to pristine graphene getting very close to its electrical, thermal and mechanical properties. The reduction of GO makes it applicable to be used in large-scale applications. Chemical reduction of graphene with hydrazine monohydrate [25] is the most established reduction procedure, which leads to reduced aqueous dispersions of graphene oxide. A disadvantage of using hydrazine as a reducing agent is the fact that it is highly poisonous and toxic. Therefore, new approaches of "green" reduction methods were investigated.

L-ascorbic acid is a colorless, odorless, crystalline, water-soluble, organic acid. The L-(+)-ascorbic acid and its derivatives with the same effect can be summarized un-

3. Results and discussion

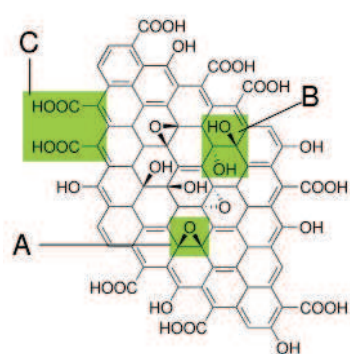


Figure 3.3.: The structure of graphene oxide [26].

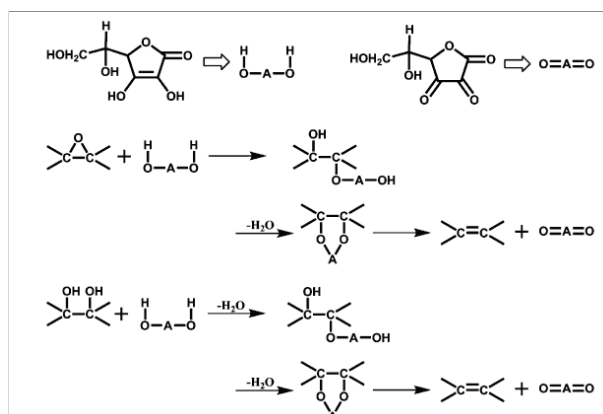


Figure 3.4.: Reduction scheme of graphene oxide [27].

der the term Vitamin C. Since ascorbic acid is easy to oxidize, it acts as a reducing agent and is used as an antioxidant. Because L-AA and its oxidized products are environment-friendly it is considered to be a "green" reducing agent. The chemical reaction during the reduction procedure is still not completely understood, but it is assumed to be a S_N2 nucleophilic reaction performed in two steps followed by thermal elimination (see figure 3.4). During the reduction process the epoxy bridges in the structure of the GO need to be opened in order to release the oxygen. ZHANG ET AL. speculate that the oxygen anion ($HOAO^-$) of L-AA breaks the $C-O$ bond considered to be the deficient electrophile and binds to it, acting as a nucleophile. This nucleophilic attack results in expelling a leaving group (H_2O). The product is an intermediate which forms reduced graphene oxide after thermal elimination. The hydroxyls of GO are removed in a similar nucleophilic reaction with oxygen anions of L-AA ($-OAO^-$) combined with the two times release of H_2O . In both reactions ascorbic acid is oxidized into dehydroascorbic acid.

The reduction was carried out on chip in L-AA solution. A first indicator of rGO was the change of color from brown (GO) to black (rGO). Figure 3.5 shows two drops of GO (left) rGO (right) where the change of color can be clearly seen. The reduction process can improve the electrical conductivity of GO by an order of magnitude. The increased charge carrier concentration and mobility will improve the reflection to incident light, which makes a rGO film have a metallic luster compared to its GO film precursor with a brown color and semi-transparency. The change of color

3.2. Physical characterization

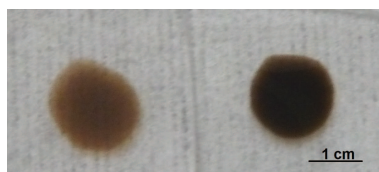


Figure 3.5.: Drop of dried GO solution (left) and rGO (right) on glass chip.

is due to an increase in the hydrophobicity of the material caused by a decrease in polar functionality on the surface of the sheets.

3.2. Physical characterization

3.2.1. Digital microscopy

In the sensor fabrication the optical characterization of the produced devices is vital. Digital microscopy is a fast technique in order to get an impression of the resulting sensor functionalization in the area of square micrometers. In this work it was mainly used for the characterization of the GO patterns fabricated via MIMIC. The production of the GO lines is highly dependent on the GO suspension and surface modification of the substrate. As stated in chapter 2.1 the GO solution was prepared by sonicating GO flakes in DI water with a concentration of 2 mg/ml. The flake size is dependent on the time used for sonication. Figure 3.6 shows a drop of GO solution after one and six hours of sonication.

The comparison shows clearly that the flakes are much smaller or even totally dispersed when sonicated for 6 hours. In order to prevent the channels to clog, the sonicated solution was left overnight so that the big flakes could settle down and the upper part was taken containing only the small flakes. Furthermore the surface of the substrate (silicon and glass chips) was silanized with APTES. Silanization occurs during the exposure of the hydroxylated substrate to the silane molecules forming a self-assembled monolayer (SAM). The silane is bound to the surface through a chemisorption process facilitating the release of the PDMS stamp from the substrate after performing MIMIC. HE ET AL. also stated that APTES prevents the aggregation of GO.

Figure 3.7 shows the result of a MIMIC experiment without silanized surface. The

3. Results and discussion

GO solution was not able to fill up the channels due to previous aggregation of the GO flakes in the channels. Furthermore residuals of PDMS stamp can be seen between the lines. The stamp itself is activated in oxygen plasma before applying it on the substrate. This is done in order to hydrophilize the stamp surface to favorable the capillary effect. The MIMIC results with the modified protocol are presented in figure 3.8.

For the characterization of GO lines silicon substrates with a 300 nm silicon oxide layer were chosen as investigated by NI ET AL. [28]. Devices for electrochemical characterization were produced on glass substrates The length of the lines is defined

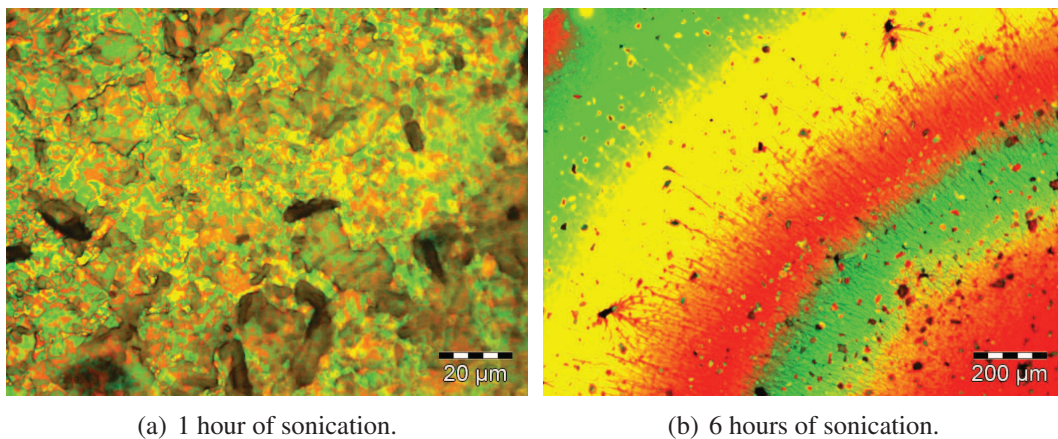


Figure 3.6.: Flake size dependence on sonication time.

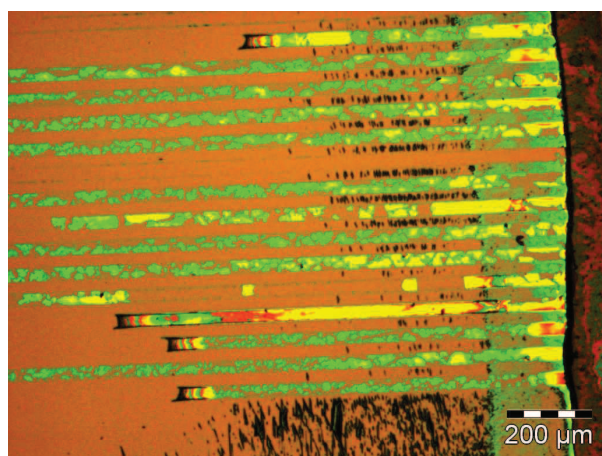
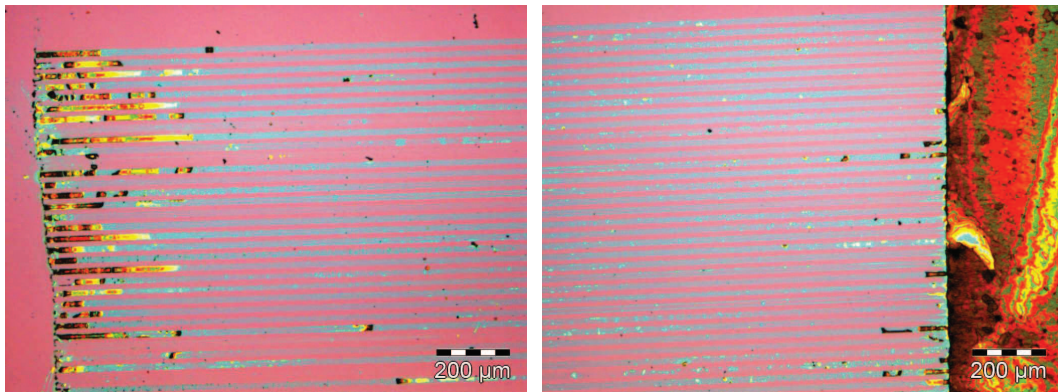


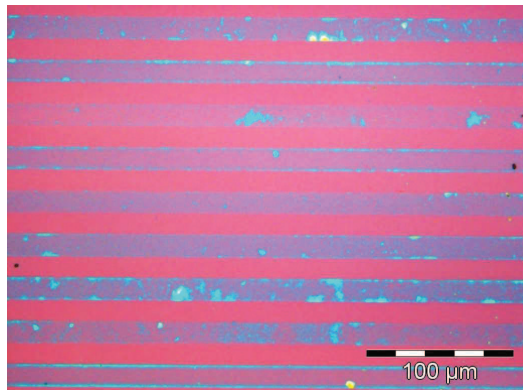
Figure 3.7.: PDMS residuals on the chip surface and aggregated GO flakes in channel resulting in discontinuous pattern.

3.2. Physical characterization



(a) End of lines.

(b) Beginning of lines.



(c) Mid of lines.

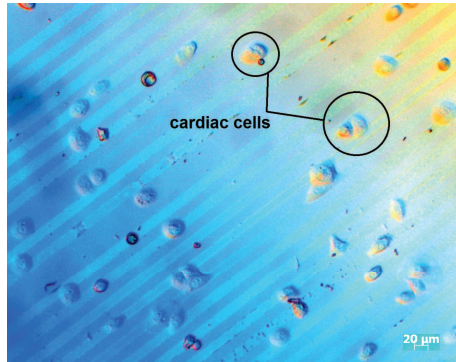
Figure 3.8.: GO pattern on silicon substrate with a width of 10 μm.

3. Results and discussion

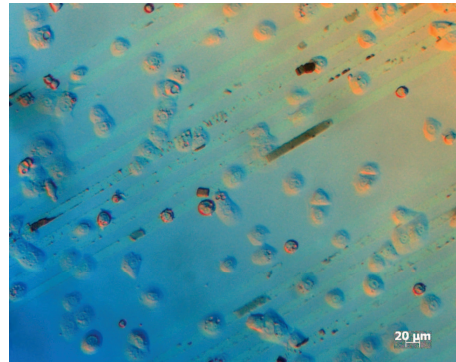
by the length of the channel, i.e. by the cutting of the stamp. The width is defined by the structure of the silicon mold used for the production of the stamp developed in a former work in our group [29]. Here it was stated that structures with a width of 10 to 30 μm gave best results. In this project it was mainly focused on lines with 10 μm width in order to compare the results with literature (see reference[30]). HE ET AL. stated in their work, that a line width between 2 and 50 μm is favorable. Too large channels would lead to aggregation of the GO flakes while smaller channels result in discontinuous GO patterns. The width of 10 μm was chosen because it is similar to the size of an animal cell.

Cell culture experiments with HL-1 cells were performed on top of the rGO lines in order to investigate the proliferation of the culture and the interface formed between cell and graphene oxide. Figures 3.9 and 3.10 show pictures of culture days 1, 4 and 7 with the comparison of two different coatings. The coating of the substrate is necessary for cell adhesion, growth, migration and differentiation [31]. For sensor applications it is not desirable, because it covers the surface leading to a decrease in sensitivity. It was attempted to study the cell growth on an uncovered surface, but no cell proliferation could be observed. Because of this fact, in this thesis the minimum thickness of the surface coating was selected. During culture time a fibronectin (figure 3.9) and a fibronectin/gelatin (figure 3.10) coating were compared. It can be stated that the cells grow on both coatings, but the substrate coated with fibronectin/gelatin is covered faster and the cell layer on culture day 7 more dense than on the fibronectin coated surface. Therefore, only the coating with fibronectin was used during the project to reduce the amount of affecting parameters.

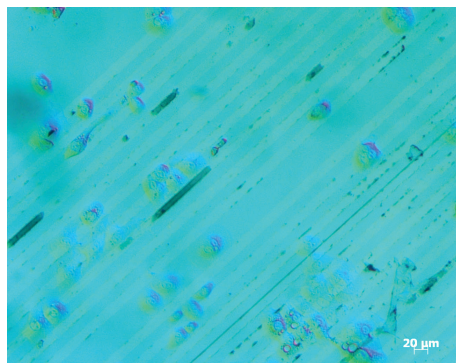
3.2. Physical characterization



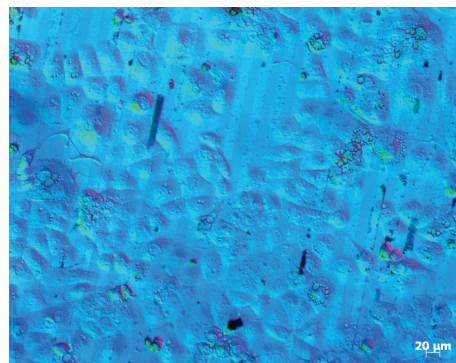
(a) Day 1, coating: fibronectin.



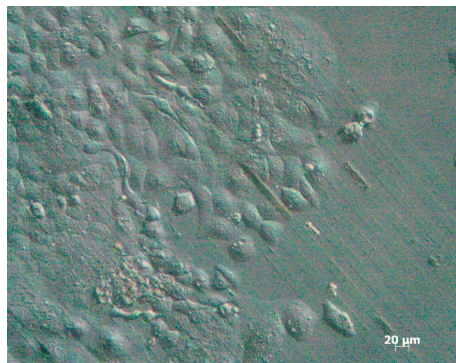
(a) Day 1, coating: fibronectin/gelatin.



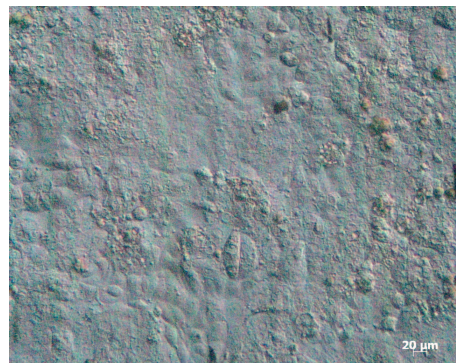
(b) Day 4, coating: fibronectin.



(b) Day 4, coating: fibronectin/gelatin.



(c) Day 7, coating: fibronectin.



(c) Day 7, coating: fibronectin/gelatin.

Figure 3.9.: HL-1 cells on rGO patterns coated with fibronectin. **Figure 3.10.:** HL-1 cells on rGO patterns coated with fibronectin/gelatin.

3. Results and discussion

3.2.2. Profilometry

Profilometry is a fast and facile technique to study the topography of surfaces. It is highly applicable for the investigation of step heights and the microroughness of processed samples. The results give a good impression of the obtained structures. In this project profilometry was used for characterization of the evaporated gold contacts and the scanning of the GO micropatterns as an additional technique to AFM measurements.

Figure 3.11 shows the height profile of the evaporated gold contact. The desired step height was 300 nm according to the protocol and showed a good correlation with the profile measurement of the gold contact. The scan of the GO lines gives an impression of the roughness on top of the lines and their height. Figure 3.12 shows the height profile of two GO patterns with a width of 20 μm . The profile shows that the width of the lines is not homogeneous from the bottom to the top. The spikes on the surface of the pattern in the graph give the impression to be very big, which is an effect of the relatively large needle tip used in the profilometer. A height of about 15 nm was achieved, which would correlate with a stacking of 15 GO monolayers. However, the profilometry method is here at its limit of resolution. Further AFM measurements confirm these results (see chapter 3.2.4). Profilometer measurements were taken with an Dektak profilometer (Veeco probe, USA)

3.2. Physical characterization

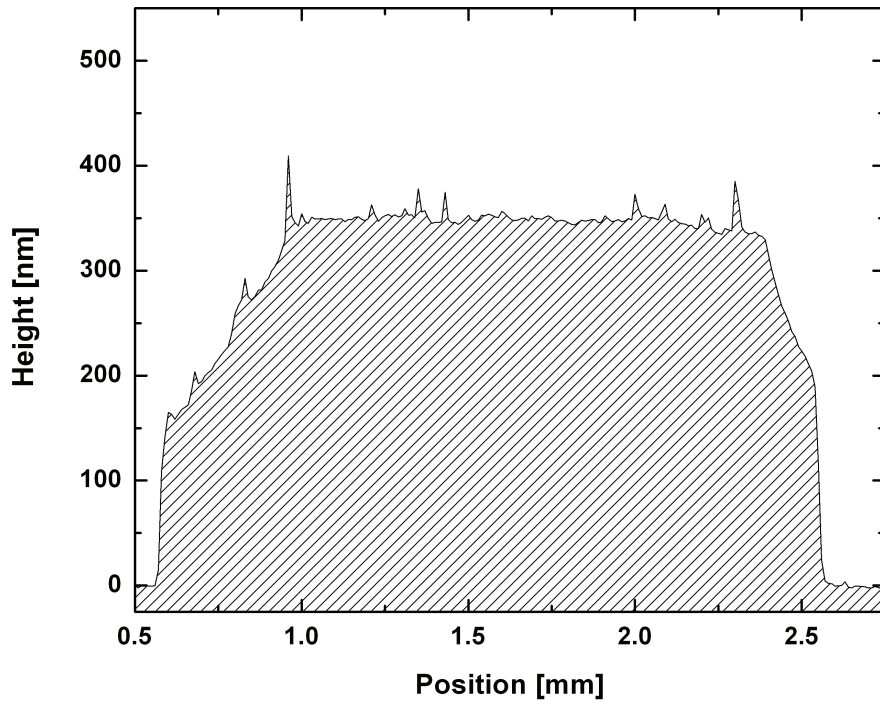


Figure 3.11.: Profilometer scan of gold contact on top of GO pattern.

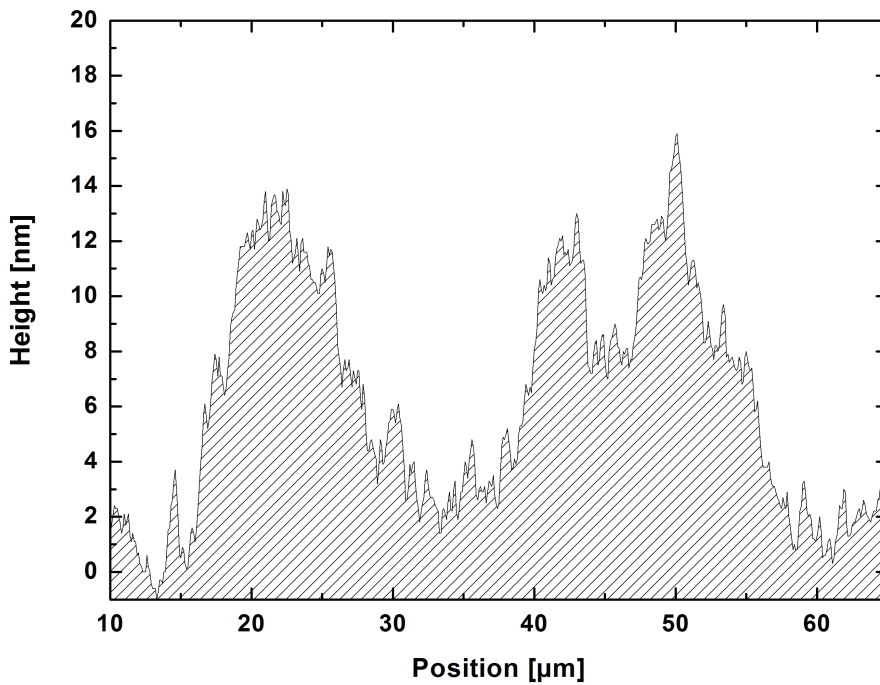


Figure 3.12.: Profilometer scan of GO patterns.

3. Results and discussion

3.2.3. Scanning electron microscopy

Furthermore the rGO patterns were characterized by SEM. Figure 3.13 shows four different SEM images zooming into the structure of the GO patterns. In figure 3.13(a) the gold contact is visible covering nicely the end of the lines. The lines are separated (see fig. 3.13(b)) and continuous. The flakes in figure 3.13(c) and 3.13(d) form a dense layer without any holes. The GO flakes stack together (darker regions) so that multilayers arise. Figure 3.13(b) depicting the GO lines expose an undefined structure on top of the patterns appearing white in the image. The same structure can be seen in the AFM image (see figure 3.14(d)). The origin of the structure could not further be investigated but is assumed to be PDMS residual. All SEM images were taken with a Zeiss Supra 40 SEM (Carl Zeiss AG, Germany).

3.2. Physical characterization

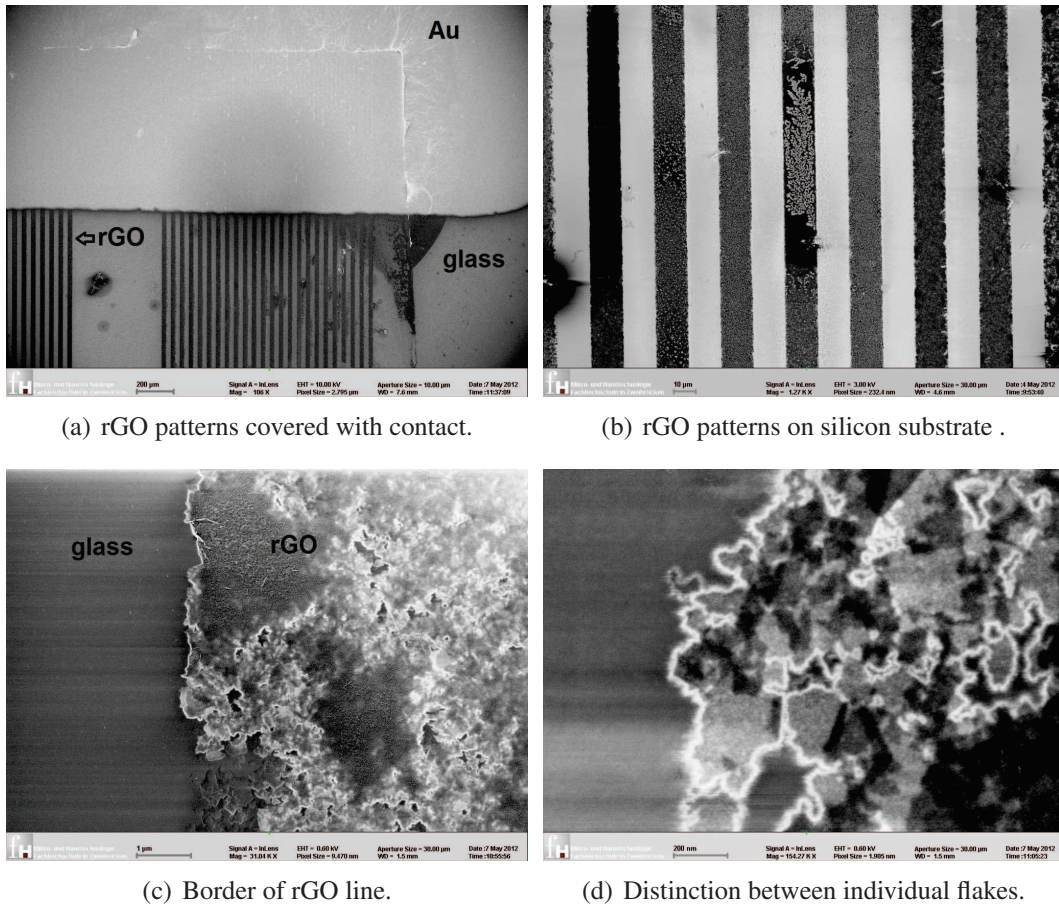


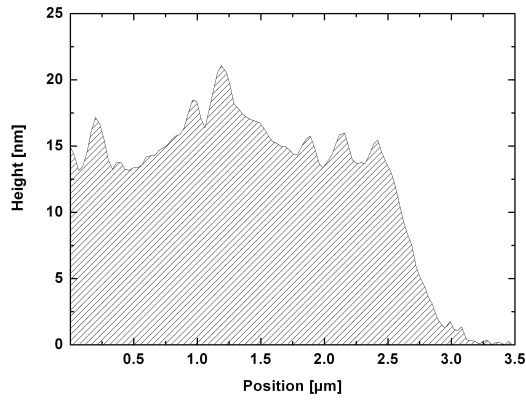
Figure 3.13.: SEM images from patterned rGO lines parallel to each other contacted with gold.

3. Results and discussion

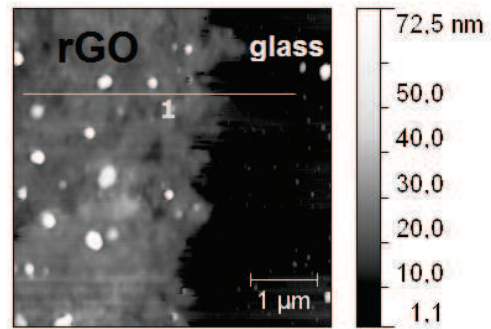
3.2.4. Atomic force microscopy

AFM images were taken in order to investigate the thickness of the rGO micropatterns. Referring to literature rGO monolayers are 1 nm thick and the thickness of single graphene sheets amounts to 0.34 nm corresponding of the interlayer spacing of graphite [32]. The rGO lines were measured in tapping mode, where the tip touches the surface only intermittently. Due to the short tip-surface contact the tapping mode prevents inelastic surface modification [33]. Figure 3.14 shows two AFM measurements of a whole rGO line (figure 3.14(c)), its border (figure 3.14(b)) and the affiliated height profiles (figures 3.14(d) and 3.14(b)). The line has a width of 10 μm . The thickness of the line amounts to 15 nm. Compared with literature the obtained thickness is 6 times higher than from HE ET AL.[30]. Here an average thickness of 2.3 nm was obtained. HE ET AL. stated that "the thickness can be easily controlled by adjusting the concentration of GO." This could not be verified. MIMIC experiments with higher (5 mg/ml) or lower (0.5 mg/ml) concentration were performed but no GO micropatterns could be obtained due to channel blocking or no visibility of the structure. All AFM images were taken with a NanoScope Dimension 3200 AFM (Veeco probe, USA).

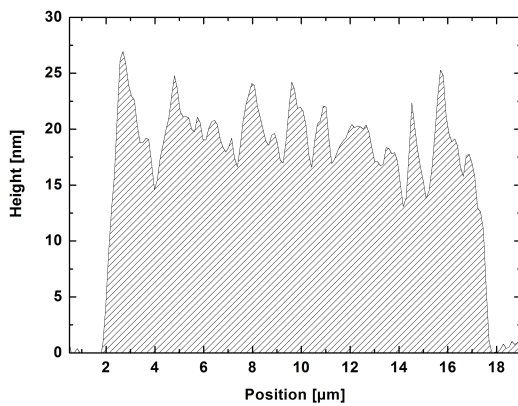
3.2. Physical characterization



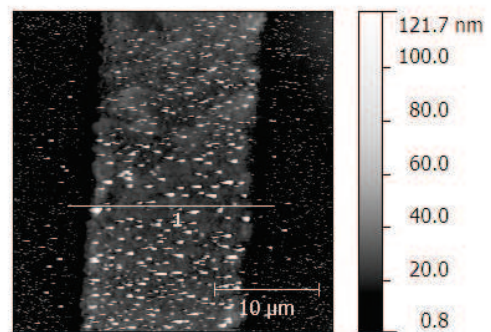
(a) Section analysis corresponding to fig. 3.14(a)



(b) Border of rGO pattern.



(c) Section analysis corresponding to fig.3.14(d).



(d) Whole rGO line.

Figure 3.14.: AFM images and section analysis of AFM data from rGO patterns on a silicon substrate with a width of 10 μm .

3.3. Electrochemical characterization

3.3.1. Impedance measurements of rGO

For the electrical characterization of the rGO micropatterns a set of parallel gold electrodes was evaporated on the rGO strips. They were used to investigate the change in impedance of the micropatterns on top of a glass chip due to the reduction of GO to rGO with L-AA. The reduction of GO (see chapter 3.1.1) is very important in order to make use of the extraordinary properties of reduced graphene oxide (see chapter 1.3.1).

The biorecognition layer is the key component of every biosensor. It defines, how sensitive and selective the biosensor is. The surface on which the biorecognition layer is deposited, has a high impact on signal detection. Impedance measurements require a material with high conductivity and a preferably low electron transfer resistance on its surface [7]. Graphene oxide can be considered as an insulator, while rGO exhibits high electrical conductivity, fast electron transfer and a large surface area. The structure of rGO contains a difference in the amount of defects and oxygen functionalities as compared to GO. During the reduction process GO changes its initial capacitive characteristics to a more and more resistive behavior. Figure 3.15 shows a Bode plot ($\log |Z|$ and phase vs. $\log f$) of an impedance spectrum before, during and after the reduction of GO. Table 3.1 shows the corresponding values of impedance and phase at 96 Hz.

Starting with unreduced GO the electrical behavior remains capacitive over the whole frequency range from 10 to 10,000 Hz (red curve). After 2 days in L-AA solution a tendency into resistive behavior is visible. The semi-resistive behavior is due to the incomplete removal of oxygen in the structure of GO. After two more days in solution total resistive behavior became apparent. This demonstrates that the reduction was successful. Impedance spectra of different sensors can be found in the appendix (section A.3).

3.3. Electrochemical characterization

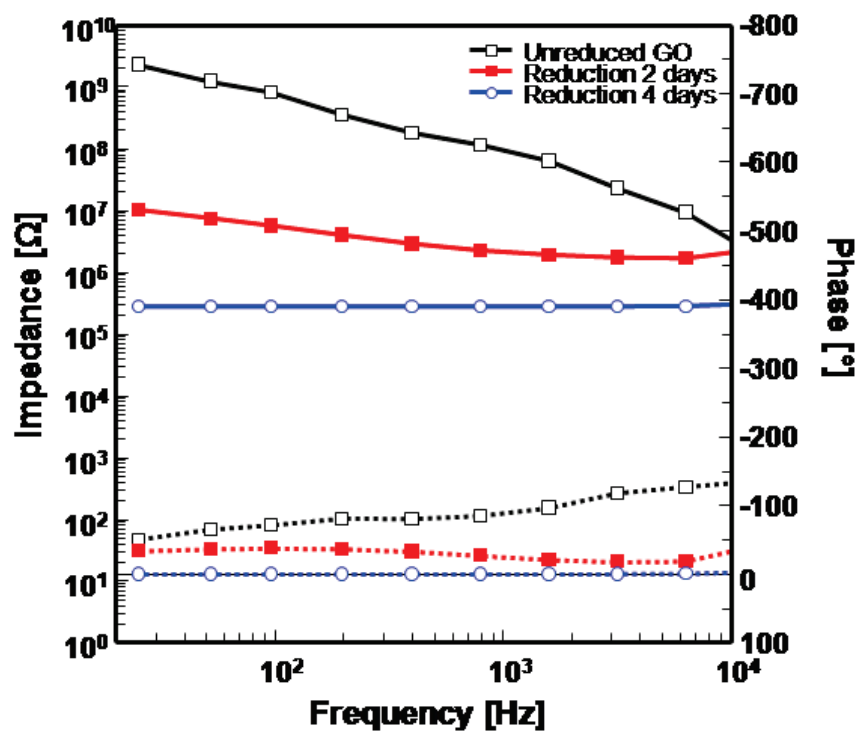


Figure 3.15.: Impedance spectrum showing the reduction progress of GO by L-AA over several days. The top curves represent the impedance amplitude and lower curves represent the phase angle. The corresponding Nyquist plot can be seen in the appendix (figure A.6).

Table 3.1.: Measured values of impedance and phase at 96 Hz before and after treatment with L-AA.

	Impedance [Ω]	Phase [$^{\circ}$]
GO	$8.2 \cdot 10^8$	-71.4
2 days	$5.6 \cdot 10^6$	-38.3
4 days	$2.7 \cdot 10^5$	-0.0

3. Results and discussion

3.3.2. Impedance measurements with functionalized sensors

Impedance measurements with biocomponents are based on the interaction of the biomolecule with the conductive or semiconductive transduction material in terms of a biological reaction that can be associated with the biological function [24]. Detection occurs by the formation of a recognition complex between the interface of the electronic transducer and analyte alternating the electrical properties of the recognition surface. Impedance spectroscopy provides resistive and capacitive properties of the recognition surface. During the characterization of a biological compound (e.g a cell layer) and the application of an ac voltage perturbation, the current has to flow through working electrode, biological material, solution and counter electrode. The resulting impedance is the sum of all individual components. Measuring the impedance behavior over a broad frequency range allows identifying the respective region where the resulting impedance is dominated by the impedance element under investigation.

For the detection of cell adsorption impedance measurements over 5 culture days were performed.

Table 3.2.: Measured values of impedance and phase at 96 Hz.

	Impedance [$M\Omega$]	Phase [$^{\circ}$]
rGO	2.1	0.0
day 1	4.2	-33.8
day 2	5.9	-36.9
day 3	5.7	-37.7
day 4	2.9	-35.9
day 5	3.4	-31.3

Figure 3.16 shows the change of impedance induced by HL-1 cells cultured on rGO patterns used as the transduction material for the biosensor and the values are given in table 3.2. Measurements were performed every 24 hours during the same time of the day. Cells were incubated on day zero. The black curve shows the resistive behavior of the unfunctionalized rGO patterns. 24 hours after cell incubation the cells had already settled down on the sensor surface. Due to the fact that a high

3.3. Electrochemical characterization

number of cells was used (700,000 cells) on 12.5 mm² the sensor surface was covered immediately. The impedance spectrum after 24 hours shows more capacitive characteristics in the measured frequency range with an increase of impedance of 100 %.

The small capacitive characteristic is based on an electrochemical double layer formed at the sensors surface, on the rGO patterns, respectively. The capacity is dependent on all compounds present at the interface, e.g. ions, solvent molecules or immobilized cells. A change in capacitance is due to a change of the dielectric constant or the thickness of the double layer [24]. The impedance spectra taken on culture day 2 and 3 show an increased impedance compared to day one (plus 40 %). The capacitance seems to be stable. Day 4 shows a decrease of impedance of about 50% remaining stable till day 5. The impedance drop on day 4 can be interpreted as a detachment of cells from the rGO pattern. Impedance spectra of a comparable

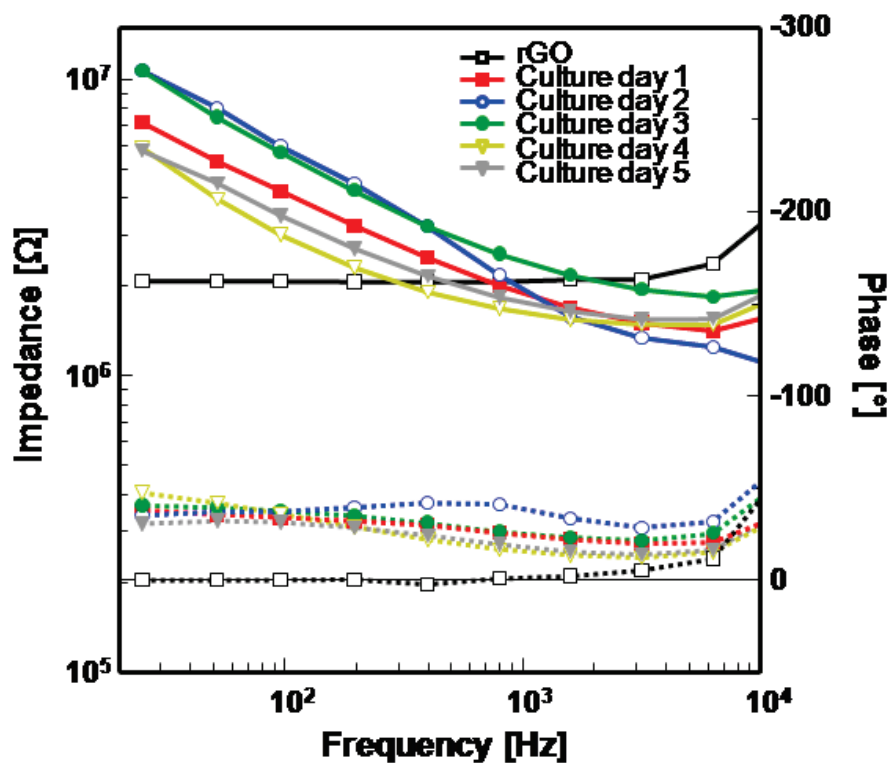


Figure 3.16.: Impedance spectrum comparing the changes in impedance due to cell adhesion over 5 culture days. The Nyquist plot of this measurement can be found in the appendix (figure A.11).

3. Results and discussion

measurement can be found in the appendix (figure A.12).

In comparison to literature, HUN YEON ET AL. [34] were developing a cytotoxicity test based on electrochemical impedance spectroscopy. Here it is stated that with an increasing amount of toxic agents, the impedance decreased due to the detachment from the electrode and a severe damage of the cells. However, in our experiment no toxic agents were used, but the area of the sensor device was limited, so that referring to the amount of cells a possible cell death could be induced by the limited space and therefore by an insufficient exchange of gases and nutrients at the sensor's surface.

3.3.3. Impedance measurements with non-adherent HL-1 cells

A second experiment under the same conditions was performed over 4 culturing days. The sensor's surface was coated with fibronectin and HL-1 cells were seeded on the rGO patterned sensing area. The encapsulated chips were incubated and measurements were performed every 24 hours. Figure 3.17 shows the impedance spectra of unfunctionalized rGO pattern, in medium, coated with fibronectin and cell functionalized rGO patterns day 1 to 4 (see legend).

It can clearly be seen, that the impedance response shows a change due to the coated surface with fibronectin. This can be explained by the formation of a protein layer on the rGO surface. The following measurements with seeded HL-1 cells did not show any further change in impedance. Microscopic images of the cell functionalized sensor surface reveal a non-adherent behavior of the cells. Comparable impedance spectra can be found in the appendix (figure A.15). Figure 3.18 shows the microscopic pictures taken over the 4 culture days. Due to the round shape of the cells it can be stated that they were not settling down on the sensor surface. In comparison to former culturing experiments (see figure 3.10) no formation of a cell layer could be observed. This can be due to a slight change in the environment or to biological variations. In comparison to figure 3.16 it can be taken as a negative control testifying that a non-adherence of cells does not influence the signal.

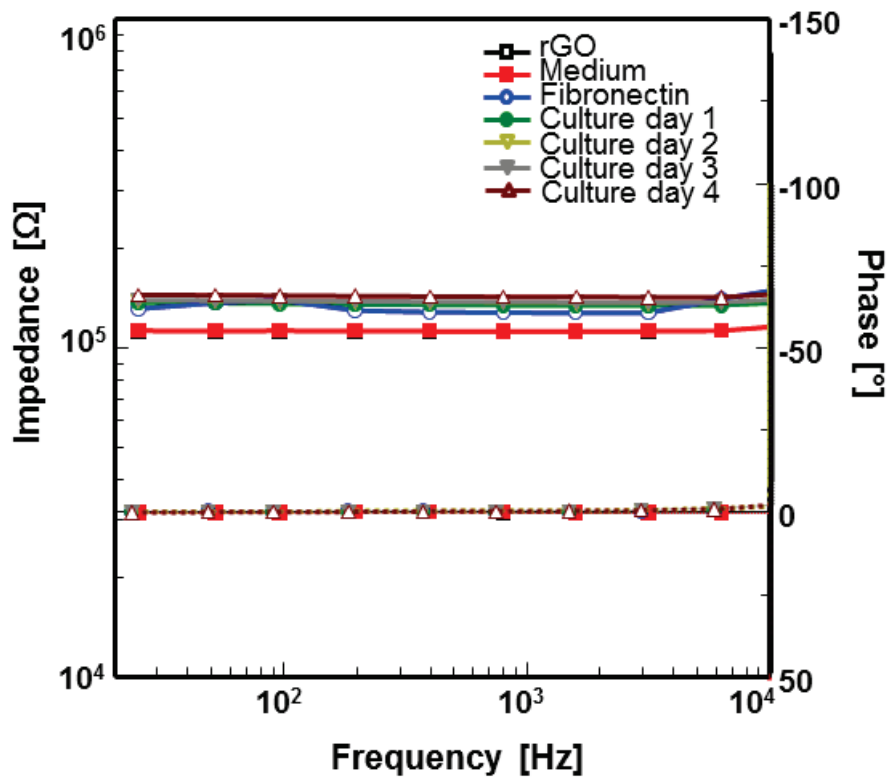


Figure 3.17.: Impedance measurements showing the spectra of a non-adherent HL-1 cells on rGO patterns. The Nyquist plot can be found in the appendix (figure A.14).

3. Results and discussion

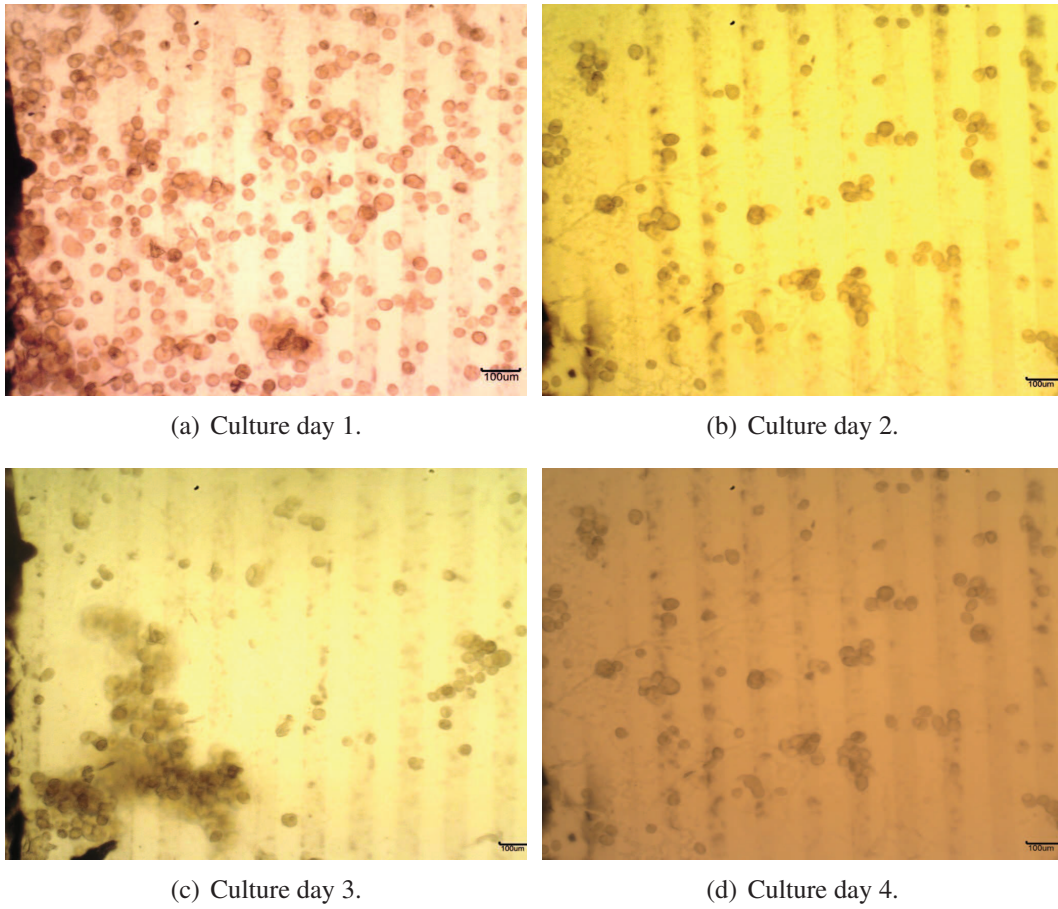


Figure 3.18.: Non-adherent HL-1 cells on sensor surface.

4. Conclusion and outlook

A graphene based biosensor interfacing electrogenic cells was developed. The sensor design was elaborated and graphene oxide was successfully implemented via soft lithography. An already established protocol of Micromolding in capillaries of a former work in our group [29] was revised and further developed through the introduction of a silanization and degassing step in the desiccator. Perfectly aligned graphene oxide patterns with μm widths and less than 20 nm heights were achieved on glass and on silicon substrates.

Physical characterization of the structured sensor surface was performed with digital microscopy, profilometry, AFM and SEM. The surface structure of the patterns was analyzed and single graphene flakes were visualized. Based on a literature study a chemical route was worked out for the reduction of graphene oxide. The obtained rGO patterns were characterized electrically with impedance spectroscopy and impedances in the $\text{M}\Omega$ range were detected. Electrogenic HL-1 cells were cultured on the sensor surface and the cell growth on the graphene patterns in response to different surface coatings was studied. Finally changes of impedance due to cell adhesion were recorded every 24 h over several culture days. Changes of impedance in the range of $2 \text{ M}\Omega$ were recorded and compared to literature.

The sensing abilities seem to be promising for sensor applications in cell-based assays including methods for cell viability, cytotoxicity and proliferation. Conventional biochemical methods such as MTT (3-(4,5-Dimethylthiazol-2-yl)-2,5-diphenyltetrazolium bromide) assays [35] are time-consuming and require multiple reagents. Additionally it is difficult to monitor the continuous behavior and real-time change of cell viability. Impedimetric techniques [34] of monitoring cell-substrate attachment and spreading of cells on the sensor surface is applicable for real-time monitoring. The sensor fabrication implementing reduced graphene oxide with soft lithography techniques is fast and cost-effective. Measurements provide shorter run

4. Conclusion and outlook

times performed on a sensitive and stable electronic transducer. To our knowledge an impedimetric technique using rGO as the transducer to measure cell adhesion has not yet been reported.

Future works should focus on scaling down the height of the rGO patterns in order to increase the sensitivity of the patterns and take advantage of graphene's properties. A different and more established protocol for the reduction of the GO lines could be investigated and compared to the one reported in this thesis. The characterization of the reduction should also be realized by Raman spectroscopy and XPS in order to gain information about the degree of reduction. Regarding to the biosensing section a further step could lead to the recording of action potentials from electrogenic cells.

Bibliography

- [1] HESS, L. H. ; JANSEN, M. ; MAYBECK, V. ; HAUF, M. V. ; SEIFERT, M. ; STUTZMANN, M. ; SHARP, I. D. ; OFFENHAEUSSER, A. ; GARRIDO, J. A.: Graphene Transistor Arrays for Recording Action Potentials from Electrogenic Cells. In: *Advanced Materials* 23 (2011), Nr. 43, S. 5045–5049
- [2] SUDIBYA, H. G.: *Nanocarbon based field effect transistors for biosensing applications*. Singapore, Nanyang Technological University, Diss., 2010
- [3] ODOM, T. W. ; LOVE, J. C. ; WOLFE, D. B. ; PAUL, K. E. ; WHITESIDES, G. M.: Improved Pattern Transfer in Soft Lithography Using Composite Stamps. In: *Langmuir* 18 (2002), Nr. 13, S. 5314–5320
- [4] KEMPAIAH, R. ; CHUNG, A. ; MAHESHWARI, V.: Graphene as Cellular Interface: Electromechanical Coupling with Cells. In: *ACS Nano* 5 (2011), Nr. 7, S. 6025–6031
- [5] NOVOSELOV, K. S.: Electric Field Effect in Atomically Thin Carbon Films. In: *Science* 306 (2004), Nr. 5696, S. 666–669
- [6] PUMERA, M.: Graphene in biosensing. In: *Materials Today* 14 (2011), Nr. 7-8, S. 308–315
- [7] BONANNI, A. ; LOO, A. H. ; PUMERA, M.: Graphene for impedimetric biosensing. In: *TrAC Trends in Analytical Chemistry* (2012), Nr. 0
- [8] HUG, T. S.: Biophysical Methods for Monitoring Cell-Substrate Interactions in Drug Discovery. In: *ASSAY and Drug Development Technologies* 1 (2003), Nr. 3, S. 479–488
- [9] XIAO, C. ; LUONG, J.: On-Line Monitoring of Cell Growth and Cytotoxicity Using Electric Cell-Substrate Impedance Sensing (ECIS). In: *Biotechnology Progress* 19 (2003), Nr. 3, S. 1000–1005
- [10] K'OWINO, I. O. ; SADIK, O. A.: Impedance Spectroscopy: A Powerful Tool for Rapid Biomolecular Screening and Cell Culture Monitoring. In: *Electroanalysis* 17 (2005), Nr. 23, S. 2101–2113
- [11] ALASTAIR H. KYLE ; CARMEL T.O. CHAN ; ANDREW I. MINCHINTON: Characterization of Three-Dimensional Tissue Cultures Using Electrical Impedance Spectroscopy. In: *Biophysical Journal* 76 (1999), Nr. 5, S. 2640–2648
- [12] LAW, J. K. Y. ; YEUNG, C. K. ; HOFMANN, B. ; INGEBRANDT, S. ; RUDD, J. A. ; OFFENHAEUSSER, A. ; CHAN, M.: The use of microelectrode array (MEA) to study the protective effects of potassium channel openers on metabolically compromised HL-1 cardiomyocytes. In: *Physiological Measurement* 30 (2009), Nr. 2, S. 155–167
- [13] ESCHERMANN, J. F. ; STOCKMANN, R. ; HUESKE, M. ; VU, X. T. ; INGEBRANDT, S. ; OFFENHAEUSSER, A.: Action potentials of HL-1 cells recorded with silicon nanowire transistors. In: *Applied Physics Letters* 95 (2009), Nr. 8, S. 083703
- [14] CATERINA SOLDANO ; ATHER MAHMOOD ; ERIK DUJARDIN: Production, properties and potential of graphene. In: *Carbon* 48 (2010), Nr. 8, S. 2127–2150

Bibliography

- [15] http://www.physik.uni-osnabrueck.de/Besucher_und_Schulen/Folien/FfF_Reichling.pdf
- [16] NOVOSELOV, K. S. ; JIANG, Z. ; ZHANG, Y. ; MOROZOV, S. V. ; STORMER, H. L. ; ZEITLER, U. ; MAAN, J. C. ; BOEBINGER, G. S. ; KIM, P. ; GEIM, A. K.: Room-Temperature Quantum Hall Effect in Graphene. In: *Science* 315 (2007), Nr. 5817, S. 1379
- [17] LIU, Y. ; DONG, X. ; CHEN, P.: Biological and chemical sensors based on graphene materials. In: *Chemical Society Reviews* (2011)
- [18] XIA, Y. ; WHITESIDES, G. M.: SOFT LITHOGRAPHY. In: *Annual Review of Materials Science* 28 (1998), Nr. 1, S. 153–184
- [19] GILLES, S.: *Nanoimprint Lithographie als Methode zur chemischen Oberflächenstrukturierung für Anwendungen in der Bioelektronik*, RWTH Aachen, Diss., 2010
- [20] http://www.ep4.ruhr-uni-bochum.de/imperia/md/content/skripte/ws05-06/physik_fuer_biologie/13teilektion_grenzfl_chen.pdf
- [21] *Action Potential*. <http://triacctionpotential.blogspot.de/>. Version: 2012
- [22] WHITE, S. M. ; CONSTANTIN, P. E. ; CLAYCOMB, W. C.: Cardiac physiology at the cellular level: use of cultured HL-1 cardiomyocytes for studies of cardiac muscle cell structure and function. In: *American journal of physiology* 286 (2004), Nr. 3, S. H823–9
- [23] HAN, Y.: *Label-free detection of biomolecules by a field-effect transistor microarray biosensor with bio-functionalized gate surfaces*. Aachen, RWTH Aachen, Diss., 2006
- [24] PÄNKE, O. ; BALKENHOHL, T. ; KAFKA, J. ; SCHÄFER, D. ; LISDAT, F.: Impedance Spectroscopy and Biosensing. In: RENNEBERG, R. (Hrsg.) ; LISDAT, F. (Hrsg.): *Biosensing for the 21st Century* Bd. 109. Springer Berlin / Heidelberg, 2008. – ISBN 978-3-540-75200-4, S. 195–237
- [25] DREYER, D. R. ; PARK, S. ; BIELAWSKI, C. W. ; RUOFF, R. S.: The chemistry of graphene oxide. In: *Chemical Society Reviews* 39 (2009), Nr. 1, S. 228
- [26] WIKIPEDIA ; WIKIPEDIA (Hrsg.): *File:Graphite oxide.svg - Wikipedia, the free encyclopedia*. http://en.wikipedia.org/wiki/File:Graphite_oxide.svg. Version: 2012
- [27] GAO, J. ; LIU, F. ; LIU, Y. ; MA, N. ; WANG, Z. ; ZHANG, X.: Environment-Friendly Method To Produce Graphene That Employs Vitamin C and Amino Acid. In: *Chemistry of Materials* 22 (2010), Nr. 7, S. 2213–2218
- [28] NI, Z. H. ; WANG, H. M. ; KASIM, J. ; FAN, H. M. ; YU, T. ; WU, Y. H. ; FENG, Y. P. ; SHEN, Z. X.: Graphene Thickness Determination Using Reflection and Contrast Spectroscopy. In: *Nano Letters* 7 (2007), Nr. 9, S. 2758–2763
- [29] KRAFT, D.: *Fabrication of graphene FET devices via MIMIC for bioelectronic applications*. Campus Zweibrücken, University of Applied Sciences Kaiserslautern, Diss., 2011
- [30] HE, Q. ; SUDIBYA, H. G. ; YIN, Z. ; WU, S. ; LI, H. ; BOEY, F. ; HUANG, W. ; CHEN, P. ; ZHANG, H.: Centimeter-Long and Large-Scale Micropatterns of Reduced Graphene Oxide Films: Fabrication and Sensing Applications. In: *ACS Nano* 4 (2010), Nr. 6, S. 3201–3208
- [31] LANSON, N. A. ; STALLWORTH, B. S. ; EGELAND, D. B. ; DELCARPIO, J. B. ; BAHINSKI, A. ; IZZO, N. J.: HL-1 cells: a cardiac muscle cell line that contracts and retains phenotypic characteristics of the adult cardiomyocyte. In: *Proceedings of the National Academy of Sciences of the United States of America* 95 (1998), Nr. 6, S. 2979–2984

Bibliography

- [32] EDA, G. ; FANCHINI, G. ; CHHOWALLA, M.: Large-area ultrathin films of reduced graphene oxide as a transparent and flexible electronic material. In: *Nature Nanotechnology* 3 (2008), Nr. 5, S. 270–274
- [33] ALESSANDRINI, A. ; FACCI, P.: AFM: a versatile tool in biophysics. In: *Measurement Science and Technology* 16 (2005), Nr. 6, S. R65–R92
- [34] JU HUN YEON ; JE-KYUN PARK: Cytotoxicity test based on electrochemical impedance measurement of HepG2 cultured in microfabricated cell chip. In: *Analytical Biochemistry* 341 (2005), Nr. 2, S. 308–315
- [35] ALBERT P LI ; CHUANG LU ; JULIE A BRENT ; CHUONG PHAM ; ANDREW FACKETT ; CHARLES E RUEGG ; PAUL M SILBER: Cryopreserved human hepatocytes: characterization of drug-metabolizing activities and applications in higher throughput screening assays for hepatotoxicity, metabolic stability, and drug–drug interaction potential. In: *Chemico-Biological Interactions* 121 (1999), Nr. 1, S. 17–35

A. Appendix

A.1. Mask layout and protocol for mold fabrication

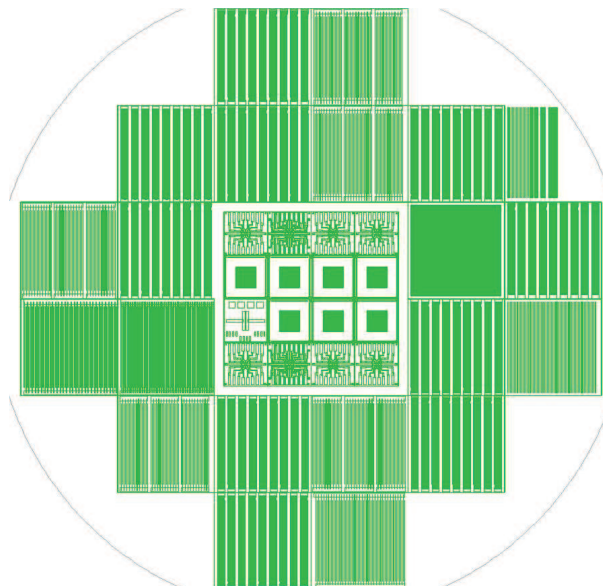


Figure A.1.: Structure of mask.

A. Appendix

Table A.1.: Cleaning of Wafer.

Step	System / Process	Material	Data
1	Caro's acid / etching sink	H_2SO_4 (conc.); H_2O_2 (30%)	124°C; 10min; ca 20-40ml H_2O_2
2	rinsing / Quick-DumpRinser	H_2O dest	5min
3	drying / RinserDryer	H_2O dest	Prog. 1: 700rpm, 3min, DI; 2000rpm, 4min, N_2

Table A.2.: Lithography.

Step	System / Process	Material	Data
4	baking out / hotplate Lanz		5min, 185°C
5	cooling down / drying cabine		RT
6	SpinCoater BLE	AR-300-80	3000rpm, 60s
7	Hotplate Lanz		185°C; 2min
8	SpinCoater BLE	AR-P 3100/10, dilution 100/40	3000rpm, 60s
9	Hotplate BLE		90°C, 2min
10	rehydration		5-10min
11	MA/BA6	mask	5.5sec; 6mW; low vacuum contact mode
12	Developer bench	AR 300-26	40s
13	Spin-dryer		2000rpm, 1min

A.1. Mask layout and protocol for mold fabrication

Table A.3.: *HF/KOH* etching.

Step	System / Process	Material	Data
1	<i>HF</i> -Dip	buffered <i>HF</i> 1,7%	20min
2	rinsing / Quick-DumpRinser	H_2O dest	6min
3	Spin-dryer		2000rpm, 30s
4	Cleaning bench	acetone; DI water; isopropanol	stripping
5	drying / Rinser Dryer	H_2O dest	700rpm, 3min; DI water; 2000rpm; 4min; N_2
6	<i>HF</i> -Dip	buffered <i>HF</i> 1,7%	30s
7	rinsing / Quick-DumpRinser	H_2O dest	6min
8	Spin-dryer		2000rpm, 30s
9	<i>KOH</i> sink		30%; 80°C; 4.5min
10	rinsing / Quick-DumpRinser	H_2O dest	3min
11	drying / Rinser Dryer	H_2O dest	700rpm, 3min; DI water; 2000rpm; 4min; N_2
12	<i>HF</i> -Dip	buffered <i>HF</i> 1,7%	30min
13	rinsing / Quick-DumpRinser	H_2O dest	6min
14	drying / Rinser Dryer	H_2O dest	700rpm, 3min; DI water; 2000rpm; 4min; N_2

A.2. Technical drawings

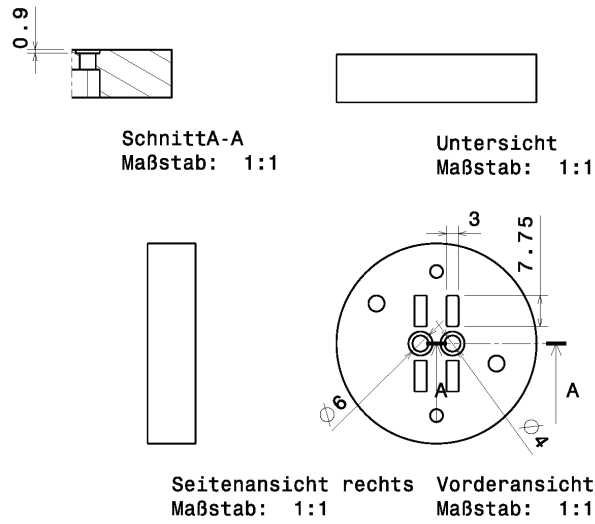


Figure A.2.: Cell 1

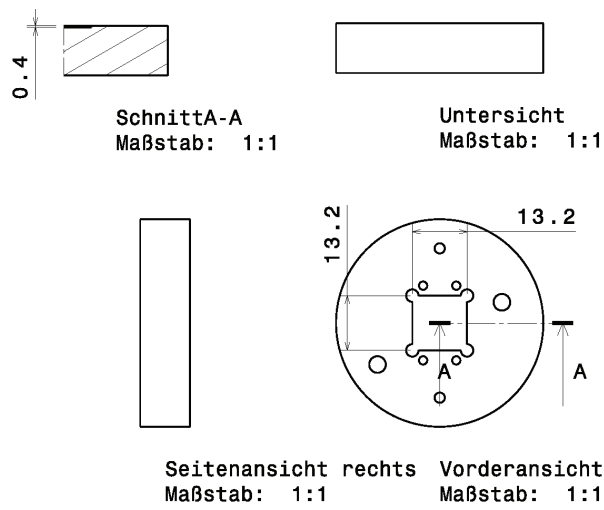


Figure A.3.: Cell 2

A.2. Technical drawings

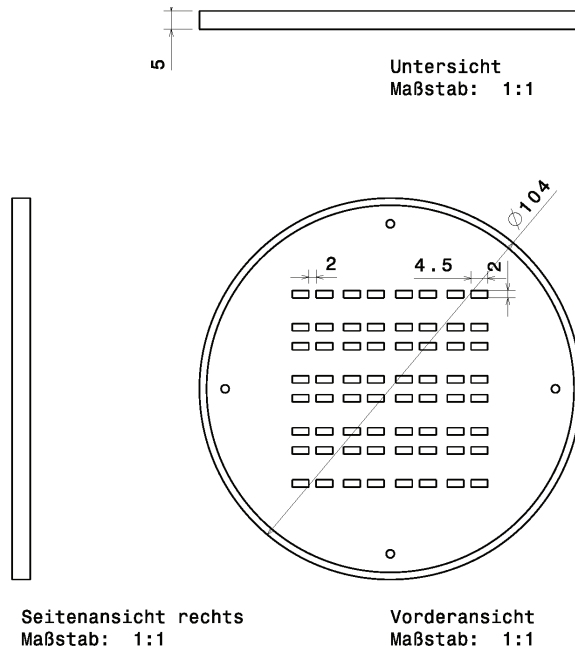


Figure A.4.: Mask 1

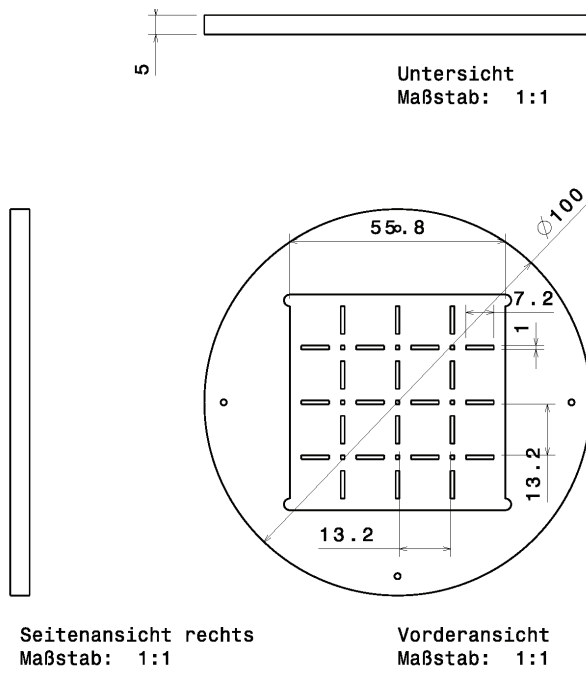


Figure A.5.: Mask 2

A.3. Impedance spectra of reduced graphene oxide

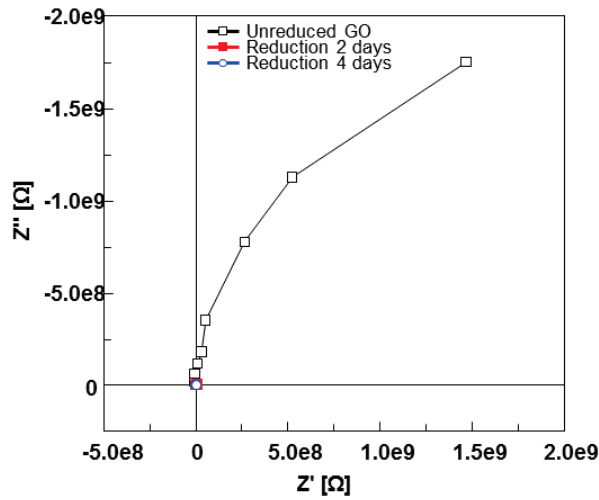


Figure A.6.: Nyquist plot of reduced graphene oxide (sensor 1).

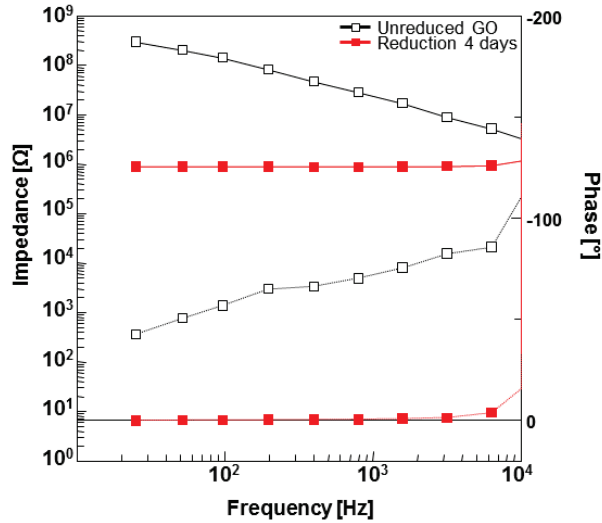


Figure A.7.: Bode plot of reduced graphene oxide (sensor 2).

A.3. Impedance spectra of reduced graphene oxide

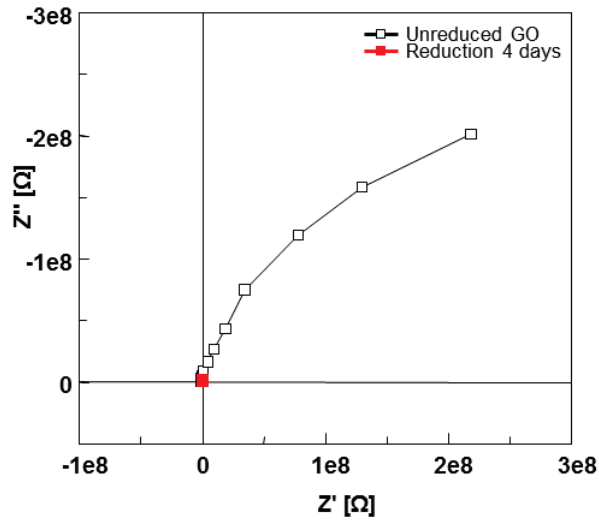


Figure A.8.: Nyquist plot of reduced graphene oxide (sensor 2).

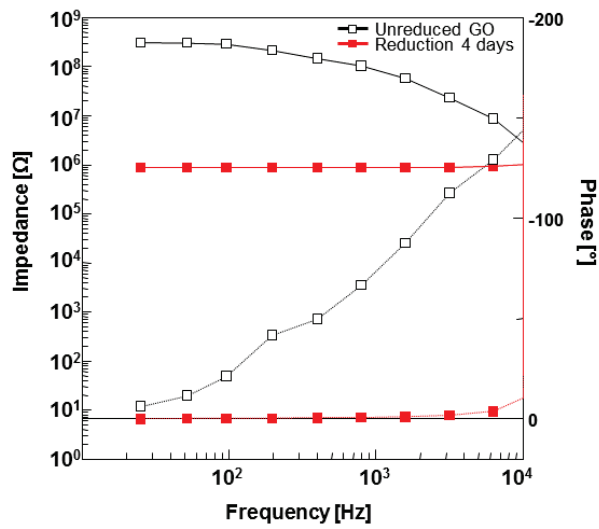


Figure A.9.: Bode plot of reduced graphene oxide (sensor 3).

A. Appendix

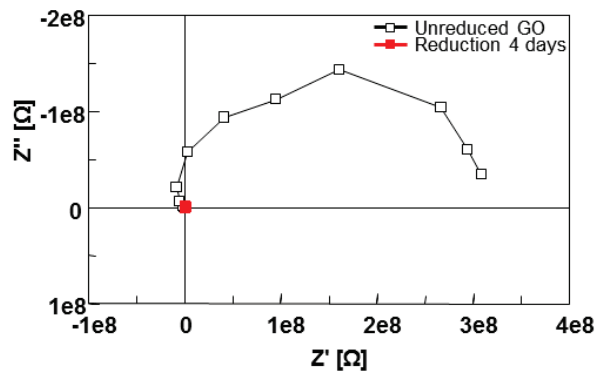


Figure A.10.: Nyquist plot of reduced graphene oxide (sensor 3).

A.4. Impedance spectra of cell functionalized sensors

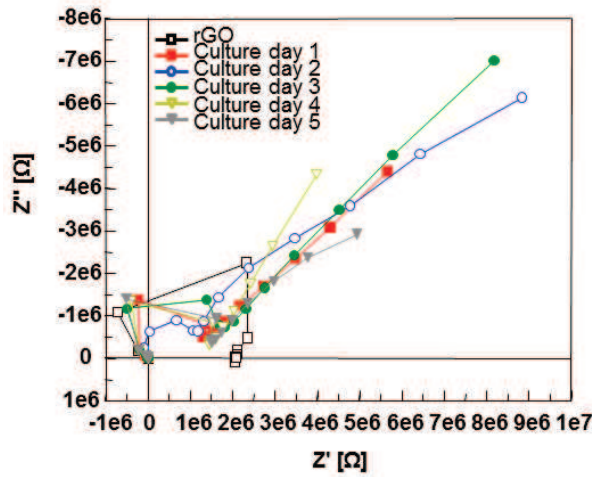


Figure A.11.: Nyquist plot of cell functionalized sensor (sensor 1).

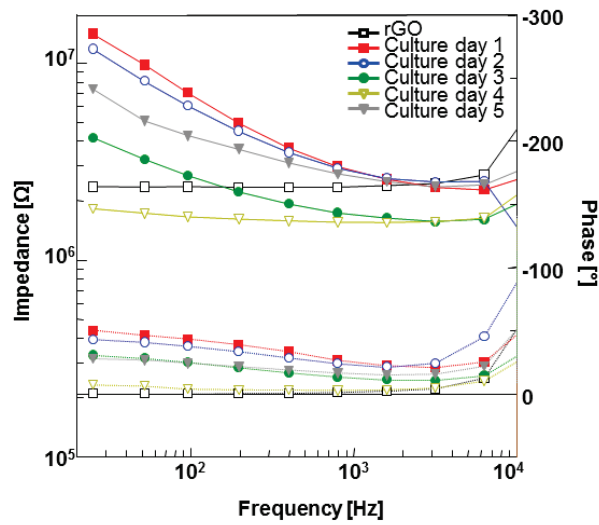


Figure A.12.: Bode plot of cell functionalized sensor (sensor 2).

A. Appendix

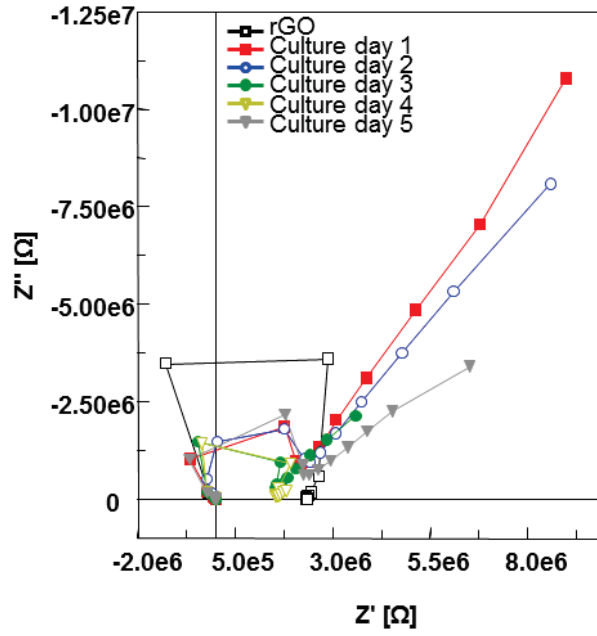


Figure A.13.: Nyquist plot of cell functionalized sensor (sensor 2).

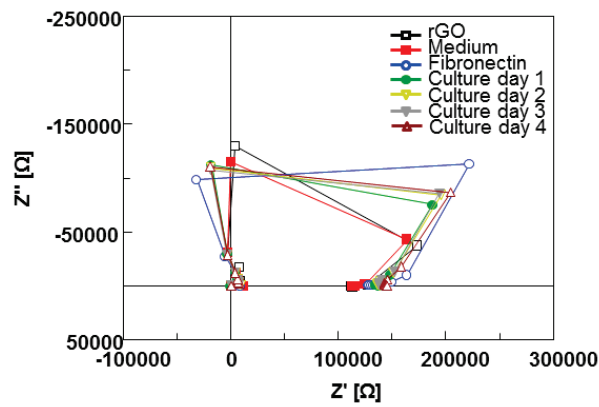


Figure A.14.: Nyquist plot of non-adherent cell functionalized sensor (sensor 1).

A.4. Impedance spectra of cell functionalized sensors

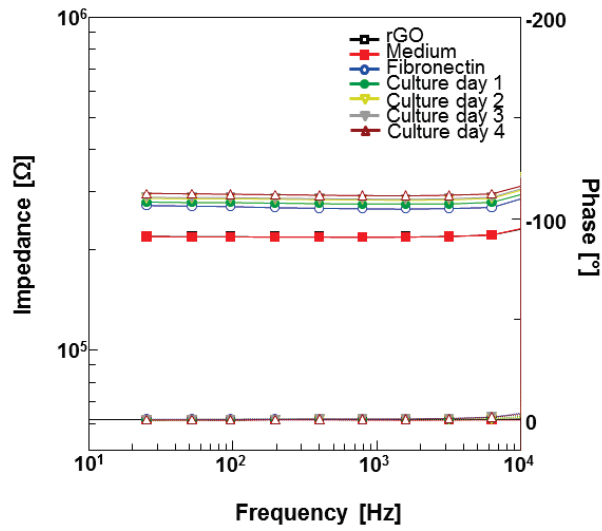


Figure A.15.: Bode plot of non-adherent cell functionalized sensor (sensor 2).

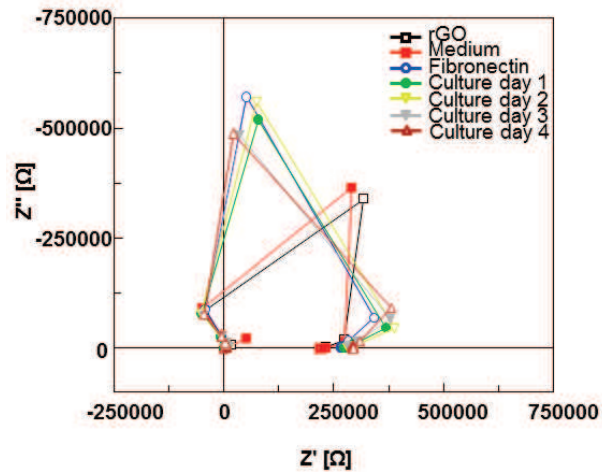


Figure A.16.: Nyquist plot of non-adherent cell functionalized sensor (sensor 2)

Acknowledgement

I would like to thank Prof. Dr. Sven Ingebrandt, Prof. Dr. Patrick Wagner and Dr. Maryam Weil for making it possible for me to join the Biomedical Signalling group at the University of Applied Sciences Kaiserslautern, Campus Zweibrücken and to do my master thesis in such an interesting interdisciplinary topic.

For the technical support I want to thank Rainer Lilischkis for the SEM measurements, Lothar Greiner for AFM measurements, Peter Molter and Detlev Cassel for the support in the cleanroom, Heike Müller and Petra Böswald for the support in the chemistry lab and Eric Engelman for the support from the mechanic factory.

My thanks also goes to the Biomedical Signalling group for the collegial atmosphere and considering me a part of the group, especially to Dr. Xuan Thang Vu for suggestions and explanations during the lab work.

A special thanks goes to my promoters Dr. Maryam Weil for her guidance and engagement during the whole project and Dr. Jessica Law for the great support during the cell culture experiments.

Last but not least I want to thank Ruben Lanche for being an good friend, colleague and flatmate.

Auteursrechtelijke overeenkomst

Ik/wij verlenen het wereldwijde auteursrecht voor de ingediende eindverhandeling:

Interfacing electrogenic cells with ultrathin layers of graphene for sensor applications

Richting: **master in de biomedische wetenschappen-bio-elektronica en nanotechnologie**

Jaar: **2012**

in alle mogelijke mediaformaten, - bestaande en in de toekomst te ontwikkelen - , aan de Universiteit Hasselt.

Niet tegenstaand deze toekenning van het auteursrecht aan de Universiteit Hasselt behoud ik als auteur het recht om de eindverhandeling, - in zijn geheel of gedeeltelijk -, vrij te reproduceren, (her)publiceren of distribueren zonder de toelating te moeten verkrijgen van de Universiteit Hasselt.

Ik bevestig dat de eindverhandeling mijn origineel werk is, en dat ik het recht heb om de rechten te verlenen die in deze overeenkomst worden beschreven. Ik verklaar tevens dat de eindverhandeling, naar mijn weten, het auteursrecht van anderen niet overtreedt.

Ik verklaar tevens dat ik voor het materiaal in de eindverhandeling dat beschermd wordt door het auteursrecht, de nodige toelatingen heb verkregen zodat ik deze ook aan de Universiteit Hasselt kan overdragen en dat dit duidelijk in de tekst en inhoud van de eindverhandeling werd genotificeerd.

Universiteit Hasselt zal mij als auteur(s) van de eindverhandeling identificeren en zal geen wijzigingen aanbrengen aan de eindverhandeling, uitgezonderd deze toegelaten door deze overeenkomst.

Voor akkoord,

Delle, Lotta

Datum: **13/06/2012**